The Journal of Physiology

The alarmin, interleukin-33, increases vascular tone via extracellular signal regulated kinase-mediated Ca^{2+} sensitization and endothelial nitric oxide synthase inhibition

Evan DeVallance[1,2], Elizabeth Bowdridge[1,2], Krista Garner[1,2], Julie Griffith[1,2], Madison Seman[1], Thomas Batchelor[1,2], Murugesan Velayutham[3], W. Travis Goldsmith[1,2], Salik Hussain[1,2], Eric E. Kelley[1,2] and Timothy R. Nurkiewicz[1,2]

[1]*Department of Physiology, Pharmacology & Toxicology, Health Sciences Center, West Virginia University, Morgantown, WV, USA*
[2]*Center for Inhalation Toxicology, West Virginia University School of Medicine, Morgantown, WV, USA*
[3]*Department of Biochemistry and Molecular Medicine, Health Sciences Center, West Virginia University, Morgantown, WV, USA*

Handling Editors: Bjorn Knollmann & Nikki Jernigan

The peer review history is available in the Supporting Information section of this article (https://doi.org/10.1113/JP286990#support-information-section).

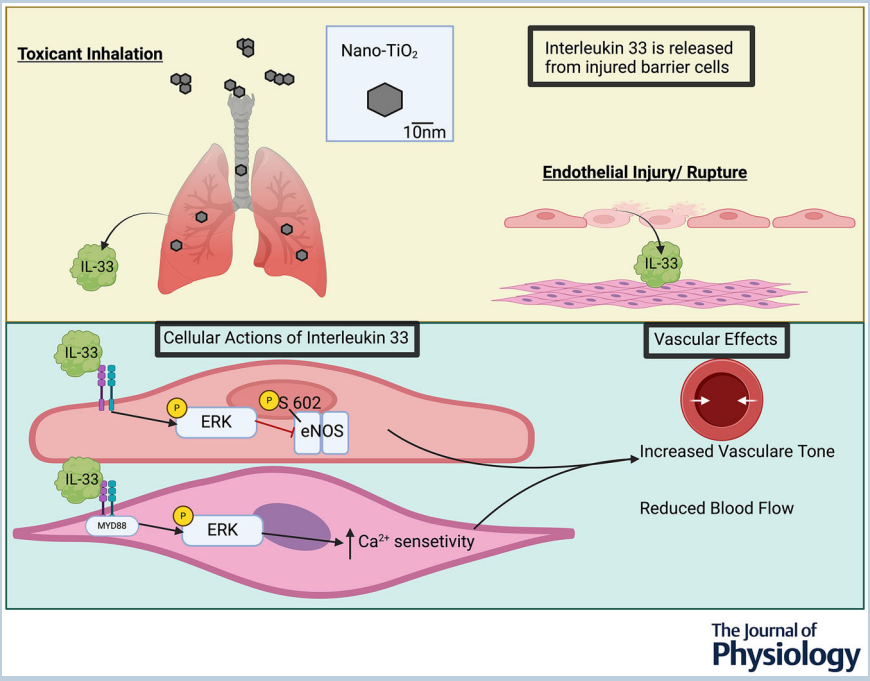

Abstract figure legend A proposed model for interleukin (IL)-33 vascular regulation is shown. Top: the known physiological sources of IL-33 as both lung and vascular injury have been reported to release IL-33. Bottom: the proposed cellular mechanism through which IL-33 acts on vascular cells. IL-33 activation of extracellular signal regulated kinase (ERK)1/2 (probably through its canonical ST2 receptor) leads to opposition of nitric oxide-mediated dilatation through inhibitory phosphorylation at serine 602. In the smooth muscle, IL-33 acting through a MyD88-ERK1/2-dependent pathway leads to increases in feed artery tone through Ca^{2+} sensitization. These actions suggest that IL-33 released from barrier cell injury acts to limit blood flow and promote healing of injured sites.

DOI: 10.1113/JP286990

Abstract Alarmins are classified by their release from damaged or ruptured cells. Many alarmins have been found to increase vascular tone and oppose endothelium-dependent dilatation (EDD). Interleukin (IL)-33 plays a prominent role in lung injury and can be released during vascular injury and in chronic studies found to be cardioprotective. Our recent work has implicated IL-33 in acute vascular dysfunction following inhalation of engineered nanomaterials (ENM). However, the mechanisms linking IL-33 to vascular tone have not been interrogated. We therefore aimed to determine whether IL-33 directly influenced microvascular tone and endothelial function. Isolated feed arteries and *in vivo* arterioles from male and female Sprague–Dawley rats were used to determine direct vascular actions of IL-33. Mesenteric feed arteries and arterioles demonstrated reduced intraluminal diameters when treated with increasing concentrations of recombinant IL-33. IL-33 activated extracellular signal regulated kinase (ERK)1/2 of rat aortic smooth muscle cells but not phosphorylation of myosin light chain kinase. This suggested IL-33 may sensitize arterioles to Ca^{2+}-mediated responses. Indeed, IL-33 augmented the myogenic- and phenylephrine-induced vasoconstriction. Additionally, incubation of arterioles with 1 ng IL-33 attenuated ACh-mediated EDD. Mechanistically, in human aortic endothelial cells, we demonstrate that IL-33-mediated ERK1/2 activation leads to inhibitory phosphorylation of serine 602 on endothelial nitric oxide synthase. Finally, we demonstrate that IL-33-ERK1/2 contributes to vascular tone following two known inducers of IL-33; ENM inhalation and the rupture endothelial cells. The present study provides novel evidence that IL-33 increases vascular tone via canonical ERK1/2 activation in microvascular smooth muscle and endothelium. Altogether, it is suggested IL-33 plays a critical role in microvascular homeostasis following barrier cell injury.

(Received 28 May 2024; accepted after revision 3 October 2024; first published online 13 November 2024)
Corresponding author T. R. Nurkiewicz: West Virginia University School of Medicine, Department of Physiology, Pharmacology, & Toxicology, 3051 Health Sciences Centre North, 64 Medical Centre Dr, Morgantown, WV 26505, USA. Email: tnurkiewicz@hsc.wvu.edu

Key points

- Interleukin (IL)-33 causes a concentration-dependent reduction in feed artery diameter.
- IL-33 acts on vascular smooth muscle cells to augment Ca^{2+}-mediated processes.
- IL-33 causes inhibitory phosphorylation of endothelial nitric oxide synthase and opposes endothelium-dependent dilatation.
- Engineered nanomaterial-induced lung injury and endothelial cell rupture in part act through IL-33 to mediate increased vascular tone.

Introduction

Interleukin (IL)-33, is a member of the IL-1 superfamily that is highly expressed in barrier cell types such as epithelial and endothelial cells (EC) (Moussion et al., 2008). IL-33 acts as an 'alarmin' released from damaged cells to initiate a type-2 immune response (Cayrol & Girard, 2014; Lefrancais et al., 2014), which has been well studied in the context of allergic responses (Cayrol & Girard, 2014). Additionally, IL-33 has been shown to be released into the circulation following pulmonary exposure to engineered nanoparticles (ENM)

Evan DeVallance is a Research Assistant Professor in the Department of Physiology, Pharmacology & Toxicology at the West Virginia University School of Medicine and is also a West Virginia Clinical and Translational Science Institute Research Scholar. Evan's primary research focus is understanding the role of redox signalling in the initiation and progression of vascular disease. He aims to integrate redox-signalling and epigenetic gene regulation to better understand cardiovascular disease risk and cardiovascular events.

(Abukabda et al., 2018; Beamer et al., 2013; Katwa et al., 2012; Wang et al., 2011) or upon EC injury (Ferhat et al., 2018). The receptor for IL-33, ST2, is expressed on both EC and vascular smooth muscle cells (VSMC) (Choi et al., 2009). IL-33 activation of its receptor in the vasculature has been studied in a chronic setting and found to be angiogenic and cardioprotective (Sanada et al., 2007). However, its acute actions on vascular function, which influence basal tone such as microvascular constriction or endothelium-dependent dilatation (EDD), are unexplored.

Nano-titanium dioxide (nano-TiO_2) is a widely used ENM and experimentally used to model ENM-induced cardiovascular impairment (Abukabda et al., 2017, 2018, 2019; Bowdridge et al., 2022; Garner et al., 2022; Nichols et al., 2018; Nurkiewicz et al., 2004; Nurkiewicz et al., 2006; Nurkiewicz et al., 2008; Nurkiewicz et al., 2009; Stapleton et al., 2013; Sun et al., 2004). Our previous work established that nano-TiO_2-induced vascular impairment is in part IL-33-dependent, through the use of an IL-33 neutralizing antibody (nAb) (Abukabda et al., 2018). However, the mechanism responsible for this finding was not examined in depth. Thus, from our previous work, it is unclear whether IL-33 is acting directly on the vasculature or indirectly through lung recruitment and activation of innate lymphoid cells and lung inflammation. Based on our previous observation and the knowledge that other alarmins acutely act on the vasculature to increase tone and alter endothelial function, we aimed to determine whether IL-33 had direct effects on feed arteries and what mechanisms mediated these responses. We therefore formed the hypothesis that IL-33 directly acts on feed arteries reducing their internal diameter and opposing EDD, thus acting to alter vascular tone and control blood flow in response to cellular damage.

Methods

Animal model

Thirty male and 10 female Sprague–Dawley (SD rats) were purchased from Hilltop Laboratories (Scottdale, PA, USA) and housed in an AAALAC accredited vivarium facility at West Virginia University under a 12:12 h light/dark photocycle at a regulated temperature. Rats used for exposure experiments were randomly assigned to either the sham-control or nano-TiO_2 exposure groups [$N = 14$; $N = 8$ male (four and four nano-TiO_2) and $N = 6$ females (three sham and three nano-TiO_2)] and acclimated to the inhalation facility for 48–72 h before initiation of inhalation exposures. Rats had *ad libitum* access to food and water throughout the acclimation period and when they in home cage before and after exposures. Animals were removed from home cages and did not have access to food or water when in the exposure chamber aiming to prevent ENM contamination of cage/bedding material, food and water. All procedures were approved by the West Virginia University Institutional Animal Care and Use Committee protocol approval #1602000621_R1.12. Rats were killed via an anaesthetic overdose (5% isoflurane 2 L min^{-1} flowrate or >600 mg kg^{-1} I.P. Inactin; Sigma-Aldrich, Inc, St. Louis, MO, USA), thoracotomy and exsanguination.

Engineered nanomaterial: nano-TiO_2

Nano-TiO_2 powder (Aeroxide TiO_2) was obtained from Evonik (Parsippany, NJ, USA). It comprises a mixture of anatase (80%) and rutile (20%) TiO_2. The particle characteristics have been determined including the primary particle size (21 nm), the specific surface area (48.08 m g^{-1}) and the Zeta potential (−56.6 mV) (Deiana et al., 2013; Suttiponparnit et al., 2011).

Nano-TiO_2 aerosols were generated using a high-pressure acoustical generator (IEStechno, Morgantown, WV, USA). The output of the generator was fed into a Venturi pump (JS-60M; Vaccon, Medway, MA, USA), which further deagglomerated the particles. The nano-TiO_2 aerosol/air mix then entered the whole-body exposure chamber. Target mass concentration (12 mg m^{-3}) was monitored in real-time with a personal DataRAM (pDR-1500; Thermo Environmental Instruments Inc., Franklin, MA, USA). Feedback loops within the software automatically adjusted the acoustic energy to maintain a stable mass concentration during the exposure. Gravimetric measurements were conducted on polytetrafluoroethylene filters (0.45 μm pore size) concurrently with the DataRAM measurements to obtain a calibration factor. The gravimetric measurements were also conducted during each exposure to calculate the mass concentration measurements reported in the study. Bedding material soaked with water was used in the exposure chamber to maintain humidity (30–70%) during exposures. Sham-control animals were exposed to HEPA-filtered air only in an identical chamber (never used for ENM exposures) with similar temperature and humidity conditions. Aerosol size distribution was determined in the exposure chamber using a scanning particle mobility sizer (SMPS 3938; TSI Inc., St Paul, MN, USA) in tandem with an aerodynamic particle sizer (APS 3321; TSI Inc.). Inhalation exposures were conducted over 3 non-consecutive days for 360 min each day. Based on: (1) prior measurements of the mass median aerodynamic diameter of the aerosol; (2) a constant mass concentration of 12 mg m^{-3}; and (3) average rat weight, we conducted aerosol deposition modelling (MPPD, version 2.11; Applied Research Associates, Inc., Albuquerque, NM, USA). This resulted in a TiO_2 alveolar lung burden of ∼82.7 μg over the three exposures. The

last exposure was conducted 1 h prior to death and experimentation.

Isolated mesenteric feed arteries

The mesenteric loop was externalized prior to death and excised immediately following heart removal (exsanguination). Second order mesenteric feed arteries were excised from the surrounding tissue and mounted on glass cannulas in a Living Systems pressure myography chamber (Living Systems Instrumentation, St Albans, VT, USA) as described previously (Abukabda et al., 2017, 2018; Bowdridge et al., 2022; Branyan et al., 2018; Brooks et al., 2015). Arteries were allowed to develop spontaneous tone, defined as the degree of constriction experienced by a blood vessel relative to its maximally dilated state. Vascular tone ranges from 0% (maximally dilated) to 100% (maximal constriction). Vessels with a spontaneous tone ≥20% of initial tone were included in this study. After equilibration, mechanisms of vasoreactivity were analysed.

Arteries were exposed to increasing concentrations of phenylephrine (PE: 10^{-10} to $10^{-6\,\mathrm{m}}$), ACh (10^{-9} to $10^{-5\,\mathrm{m}}$), sodium nitroprusside (SNP) (10^{-9} to 10^{-4} M) and IL-33 (0.001–100 ng mL^{-1}), which were each added separately to the bath. Additionally, vessels were incubated with 1 ng mL^{-1} IL-33 or 5 μM of the extracellular signal regulated kinase (ERK) inhibitor FR180204 before reperforming PE, ACh and SNP curves. The steady-state diameter of the vessel was recorded for at least 2 min after each dose. After each dose curve was completed, the vessel bath was exchanged to remove excess chemicals by carefully removing the superfusate and replacing it with fresh warmed oxygenated physiological saline solution (PSS). After all experimental treatments were complete, the PSS was replaced with Ca^{2+}-free PSS until maximum passive diameter was established.

Myogenic response in feed arteries (±1 ng mL^{-1} IL-33 incubation and/or air embolus) was assessed by monitoring internal diameter for 3 min at lumen pressures in 20 mmHg increments from 20 mmHg to 120 mmHg normalized to passive vessel diameter as above. Additionally, the myogenic index was calculated using:

$$\text{Myogenic index} = \frac{\left\{\frac{\Delta D}{Dp}\right\}}{\Delta P} \times 100$$

where ΔD is the change in diameter for a given pressure, Dp is the previous diameter and ΔP is the change in pressure.

Spontaneous tone was calculated using:

$$\text{Spontaneous tone}\ (\%) = \left\{\frac{(m - Di)}{Di}\right\} \times 100$$

where Dm is the maximal diameter and Di is the initial steady-state diameter recorded prior to the experiment.

The experimental responses to ACh and SNP are expressed using:

$$\text{Diameter}\ \left(\%\ \text{maximal response}\right) = \left\{\frac{(Dss - Dcon)}{(Dm - Dcon)}\right\} \times 100$$

where $Dcon$ is the control diameter recorded prior to the dose curve and Dss is the steady-state diameter at each dose of the curve. The experimental response to PE and IL-33 are expressed using:

$$\text{Diameter}\ (\%\ \text{of initial diamter}) = \left\{\frac{(Dcon - Dss}{Dcon - D\mu}\right\} \times 100$$

where $D\mu$ is the unpressurized minimal diameter

Pin myography

Aortic rings were sectioned from the thoracic aorta and hung on pins in a Danish Myo Technology (DMT) system containing a physiological salt solution. The rings were pre-stretched to optimal tension based on the DMT protocol (https://www.dmt.dk/uploads/6/5/6/8/65689239/dmt_normalization_guide.pdf) then equilibrated for 1 h. EDD was then tested by pre-constriction with 10^{-6} PE and then increasing concentrations of ACh as in the pressure myography experiments. EDD was calculated as a percentage from the pre-contracted tension:

$$\text{Relaxation}\ (\%\ \text{contraction}) = \frac{(TSS - Ti)}{(Tpe - Ti)} \times 100$$

where TSS is the stead state tension at each dose of the drug response, Ti is the initial baseline tension, and Tpe is the steady-state tension of the PE pre-contraction.

Intravital microscopy

Rats were anaesthetized with Inaction (100 mg kg$_{-1}$, supplemented as needed) and placed on a heating pad to maintain 37°C measured by rectal temperature. The airway was kept patent by intubation and the right carotid artery was cannulated to measure arterial pressure. Next, an incision on the ventral midline just below the ribs was made to expose the abdominal cavity. Then, a 16–20 cm section of the ileum was externalized, small incisions were made to flush the section of chyme and then sutures were placed to stretch the mesenteric loop over the optical platform. The stage/optimal platform was continuously superfused with warmed electrolyte solution

(119 mM NaCl, 25 mM $NaHCO_3$, 6 mM KCl and 3.6 mM $CaCl_2$), supplemented with isoproterenol (10 mg L^{-1}) and phenytoin (20 mg L^{-1}) to inhibit the peristaltic motion of the intestine and equilibrated with 95% N_2 and 5% CO_2. Superfusate was maintained at a flow rate between 4 and 6 mL min^{-1} to minimize atmospheric oxygen equilibration. At this time, the animal and platform were transferred to the microscope platform for experimental visualization using a BX51W1 microscope with a DP71 camera (Olympus, Tokyo, Japan). IL-33 was delivered at the indicated concentrations (0.01 ng mL^{-1} to 10 ng mL^{-1}) via a mechanical syringe pump. Digital photomicrographs were captured at steady-state response and the internal diameter was measured using ImageJ (NIH, Bethesda, MD, USA) and presented as μm change in diameter.

Cell culture

Human aortic endothelial cells (HAEC; CC-2535) were purchased from Lonza (Walkersville, MD, USA) and used between passages 3–7. HAEC were grown in complete EBM media containing EGM bullet kit (CC-3182; Lonza) and serum-synchronized in 1:10 serum reduced EBM media for 4 h prior to treatments. Cells were then treated with the indicated concentration of recombinant human IL-33 for the indicated time points. At this point, the cell media was collected and the cells were washed and collected in RIPA for western blot or assay buffer was added to conduct oxidant or nitric oxide experiments. For generation of culture media for isolated vessels, HAEC cells were plated on 10 cm dishes and grown to confluency and then switched to 1:10 serum reduced EBM media overnight. The next morning, cells were mechanically disrupted with a sterile P1000 pipette tip or sham (the media was stirred with a P1000 pipette tip but cells were not contacted). The media was collected and then centrifuged at 1000 rpm (∼200 *g*) for 5 min at 4°C to remove insoluble cellular debris aliquoted and snap frozen. The media aliquot was then thawed and kept on ice until use in the isolated vessel experiments at the indicated volumes.

Rat aortic smooth muscle cells (RASMC) were grown in Lonza smooth muscle complete media (Lonza, Basel, Switzerland) as previously described (Bowdridge et al., 2022). RASMC were plated ina six-well or clear bottom black-sided 96-well plate and serum starved for 24 h prior to the experiments. Cells were exposed to 1 ng mL^{-1} IL-33 for 10 min then collected for western blot or 96-well plates fixed for in-cell western assays. ST2 neutralization was conducted in HAEC, pretreating with 0.8 μg mL^{-1} ST2 nAB (R&D systems, Minneapolis, MN, USA) for 30 min prior to treating the cells with 1 ng mL^{-1} IL-33 for 10 min.

Western blots

Samples were prepared with laemmli sample buffer and β-mercaptoethanol and run on a 4–20% gradient gel (Bio-Rad, Hercules, CA, USA) at 70 V. Samples were then transferred to 0.45 μm nitrocellulose membranes, dried, reconstituted with $ddiH_2O$. Membranes were blocked with Li-Cor (Lincoln, NE, USA) Tris-buffered saline (TBS) blocking buffer and incubated in primary antibody overnight at 4°C. Primary antibodies include β-actin (dilution 1:1000; Santa Cruz Biotechnology, Dallas, TX, USA), phosphorylated and total ERK1/2 (dilution 1:1000; Cell Signaling Technology, Danvers, MA, USA), S602-phosphorylated-endothelial nitric oxide synthase (eNOS) (dilution 1:500; Thermo Fisher Scientific, Waltham, MA, USA), eNOS (dilution 1:1000; Cell Signaling Technology) phosphorylated-Rho associated coiled-coiled containing kinase (ROCK2) (dilution 1:500; GeneTex, Irvine, CA, USA), phosphorylated-calmondulin-dependent kinase (CaMK) (dilution 1:500; GeneTex) and phosphorylated myosin light chain (MLC) (in-cell western dilution 1:200, traditional western dilution 1:750; Cell Signaling Technology). In Fig. 2, total protein was used as the loading as measured using a Revert 700 stain (Li-Cor) Membranes were then washed with TBS containing 0.1% tween (TBST), incubated in Li-Cor near-infrared secondary antibodies for 1 h at room temperature, washed again with TBST and finally imaged with the Li-Cor Odyssey Clx. Densitometry analysis was conducted in ImageJ (NIH) reported as target normalized to β-actin and fold change calculated from control.

In-cell western assay. The in-cell western assay was conducted as described previously (Bowdridge et al., 2022), in 96-well plates in accordance with the Li-Cor protocol. In brief, cells were fixed and permeabilized with 2% paraformaldehyde and 0.01% Triton X. Cells were then blocked with Li-Cor blocking buffer for 1.5 h and then primary antibody was added at 1:100 dilution and rocked at room temperature for 2 h. The plate was then washed with TBST five times and then the Li-Cor second antibody CW800 with Li-Cor CellTag 700 was added, followed by incubation for 1 h. Finally, the plate was washed five times and the plate was imaged on the Li-Cor Odyssey Clx with a focus offset of 3 mm.

Oxidant production

Electron paramagnetic resonance (EPR) spectrometry. HAEC were loaded with 0.2 mM of 1-hydroxy-3-methoxycarbonyl-2,2,5,5-tetramethylpyrrolidine hydrochloride (CMH) (catalog no. ALX-430-117; Enzo Life Science, Farmingdale, NY, USA) and then treated with 10 ng mL^{-1} IL-33. The reaction was allowed to incubate

for 30 min at 37°C ± superoxide dismutase (SOD). After 30 min, the cells and media were collected and snap frozen. At the time of EPR measurements, frozen samples were rapidly thawed, loaded (50 μL) into a glass capillary tube (Ref: 9600150; Hirschmann Laborgerate GmbH & Co. KG, Eberstadt, Germany), sealed on one end using Critoseal clay (VWR, Radnor, PA, USA) and placed inside the 4 mm (outer diameter) EPR quartz tube (catalog. no. 707-SQ-250M; Wilmad LabGlass, Vineland, NJ, USA). EPR spectra were recorded at room temperature usinng a EMXnano spectrometer (Bruker, Billerica, MA, USA) operating at X-band with a 100 kHz modulation frequency. The following EPR instrument parameters were used: microwave frequency, 9.617 GHz; centre field, 3425 G; sweep width, 100 G; microwave power, 20 mW; modulation amplitude, 1 G; modulation frequency, 100 kHz; receiver gain, 50 dB; time constant, 10.24 ms; conversion time, 30 ms; sweep time, 30 s; number of scans, 1. Data acquisition was performed using Xenon-nano software (Bruker). The signal intensity was measured using first peak (low field) height of the EPR spectrum.

Coumarin boronic acid (CBA) assay. A CBA assay was conducted as described previously (Bowdridge et al., 2022; de Jesus et al., 2019; DeVallance et al., 2019, 2022; Li et al., 2019, 2021; Novelli et al., 2019). For 96-well plates; cell culture media was removed and 100 μL of CBA buffer added [Hanks balanced salt solution, ± L-NAME (Sigma-Aldrich, St Louis, MO, USA), taurine (Sigma-Aldrich) and 500 μM CBA probe (Cayman, Ann Arbor, MI, USA) ± 1 KU catalase (Sigma-Aldrich, St)]. Plates were then run in a 37°C plate reader and fluorescence measured (excitation 350, emmission: 450; Spectramax M2 plate reader; Molecular Devices, San Jose, CA, USA) every 1 min over 2 h. Signals from the negative control catalase wells were subtracted out from the sample wells and only the catalase inhibitable signal was analysed. The rate of the relative fluorescence units per minute was calculated for all samples and the fold change from control treatment was calculated.

Cytochrome *c*. Superoxide ($O_2^{\bullet-}$) production was measured in HAEC lysates. Briefly, HAEC were washed twice with ice-cold PBS, then cells were scraped in ice-cold disruption buffer (Ghouleh et al., 2017) and underwent a freeze–thaw cycle, which was followed by a needle pass. Lysates were centrifuged at 1000 ***g*** for 10 min at 4°C and the supernatant was collected. Homogenates containing the membrane fractions (10 μg per well) were added to assay buffer (65 mM sodium phosphate buffer, pH 7.0, 1 mM EGTA, 180 μM NADPH, 10 μM FAD, 1 mM $MgCl_2$, 2 mM NaN_3, 0.2 mM cytochrome *c* ± 50 U of superoxide dismutase) and $O_2^{\bullet-}$ was measured as the SOD-inhibitable rate of cytochrome *c* reduction quantitated at 550 nm (Spectramax M2 plate reader; Molecular Devices).

Nitrate/nitrite

Measurement of nitrate/ nitrite in culture media was used as a surrogate for nitric oxide production. HAEC were washed and changed to basal EBM media without serum (serum contains nitrate compounds) and pretreated with 10 ng mL^{-1} IL-33 ± 5 μM FR180204 for 60 min and then HAEC stimulated with 20 μM A23187. The cell culture media was collected following 60 min of incubation and snap frozen. Next, 20 μL of HAEC culture media was injected in triplicate into the reaction chamber (NOA 280i SIEVERS, GE, Chicago, IL, USA) to measure NO. The reaction occurred in saturated vanadium chloride (VCl_3, 0.8 g per 100 mL) filled heated purge vessel (∼90°C), bubbled with inert N_2. Produced NO enters a NaOH trap and analysed by the chemiluminescence analyser (NOA 280i; SIEVERS, GE, Chicago, IL, USA). The measurement from the triplicates were averaged to generate a sample's mean NO. Media from non-stimulated HAEC was used as a negative control. The fold change in signal was taken compared to the vehicle treated, stimulated HAEC.

Statistical analysis

Data are expressed as the mean ± SEM. Point-to-point differences in the concentration response curves were evaluated using two-way repeated measures ANOVA with Holm–Sidak *post hoc* analysis when significance was found. The ERK time course was analysed using a one-way repeated measures ANOVA with Holm–Sidak *post hoc* analysis when significance was found. Effects of ERK inhibition in cultured endothelial cells analysed by one-way ANOVA with Holm–Sidak *post hoc* analysis when significance was found. Student's *t* test was utilized for comparison between two groups. All statistical analysis was completed with Prism (GraphPad Software Inc., San Diego, CA, USA). $P < 0.05$ was considered statistically significant. *N* is the number of animals per group and *n* is the number of vessels per group.

Results

IL-33 increased vascular tone

Isolated second order mesenteric feed arteries (Table 1) incubated with increasing concentrations of IL-33 showed a significant reduction in intraluminal diameter from baseline at the concentration of 0.1 ng mL^{-1} and above compared to the same concentration of heat-denatured IL-33 control (0.1 ng mL^{-1}, $P < 0.01$; 1 ng mL^{-1},

Table 1. Characteristic of second order feed mesentery feed arteries

	N (*n*)	Lumen diameter @ 70 mmHg (μm)	Outer diameter @ 70 mmHg	% Tone
Sprague–Dawley Mesentery arteries	26 (*n* = 43)	235.9 ± 38.6	278.2 ±39.9	24.8 ± 2.4
Vessels used for Pe Or ACh curves	Baseline, *n* = 12	245.9 ± 25.7	–	–
	1 h IL-33 incubation, *n* = 12	239.2 ± 21.2	–	–
		P = 0.206		

Data represented as the mean ± SD. *N* is the number of animals and *n* is the number of vessels.

$P < 0.01$; 10 ng mL^{-1}, $P < 0.01$) (Fig. 1*A*). Furthermore, this IL-33 response could be prevented by inhibition of MyD88 with 100 μM TJ-M2010 (0.1 ng mL^{-1}, $P < 0.01$; 1 ng mL^{-1}, $P < 0.01$; 10 ng mL^{-1}, $P < 0.01$) (Fig. 1*A*). As vascular responsiveness is known to differ between male and female, we next isolated both male and female mesenteric feed arteries and exposed them to increasing concentrations of IL-33. The response demonstrated no

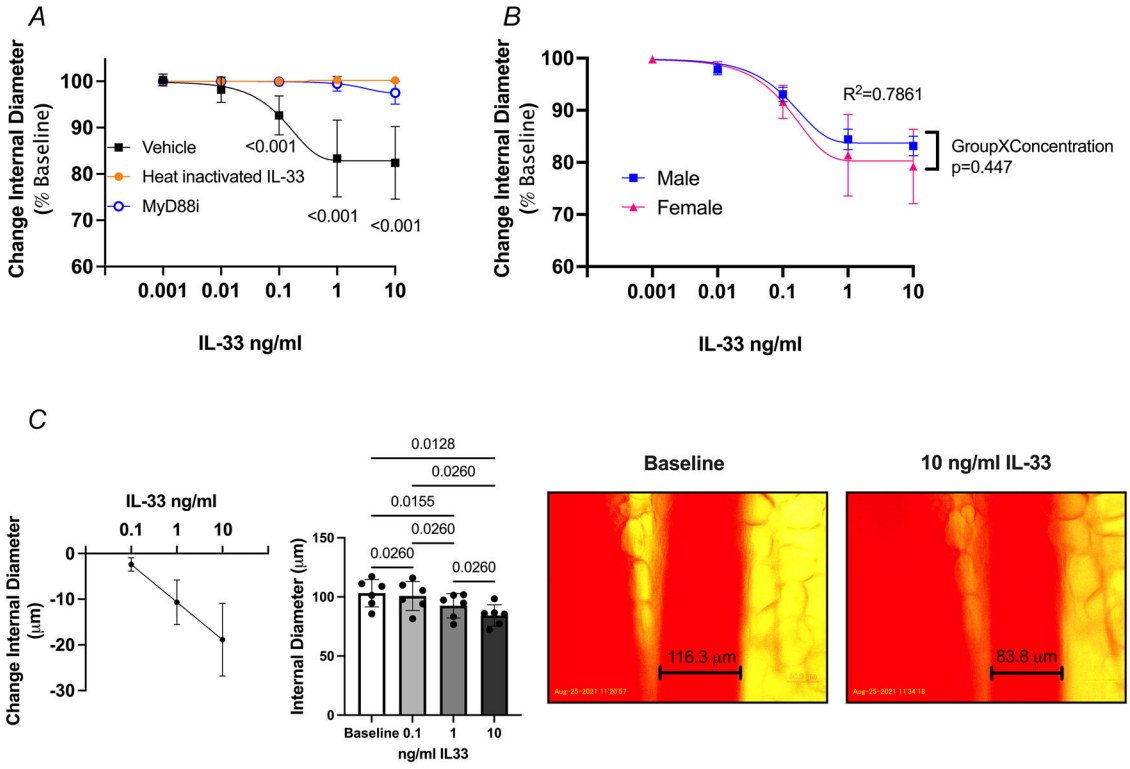

Figure 1. IL-33 reduces feed artery lumen diameter
A, pressurized mesenteric feed arteries from Sprague–Dawley rats exposed to increasing concentration of IL-33, heat-inactivated IL-33 or IL-33 following Myd88 inhibition ($N = 6$, $n = 12$). Analyzed by two-way repeated measures ANOVA (Group × Concentration, $P < 0.001$) with Holm–Sidak *post hoc* analysis, which shows $P < 0.001$, vehicle *vs*. heat-inactivated and Myd88 at the indicated concentrations. *B*, IL-33 response was not sex-specific (male: $N = 5$, $n = 9$; females: $N = 4$, $n = 7$) analysed by two-way repeated measures ANOVA (Sex × Concentration, $P = 0.447$). A goodness of fit analysis of the whole data set has an $R^2 = 0.786$. *C*, intravital microscopy assessment of mesenteric arterioles exposed to IL-33 in anesthetized Sprague–Dawley rats ($N = 6$, $n = 6$). Data are represented as the change in internal diameter and raw internal diameter at baseline and each concentration of IL-33 analysed by one-way repeated measures ANOVA with Holm–Sidak *post hoc* analysis, which shows a concentration-dependent decrease in lumen diameter: baseline *vs*. 0.1 ng mL^{-1} IL-33, $P = 0.0260$, 0.1 *vs*. 1 ng mL^{-1} IL-33, $P = 0.0260$ and 1 *vs*. 10 ng mL^{-1} IL-33, $P = 0.0260$. Data are the mean ± SD; individual data points and full statistical analysis can be found in the Supplemental data. [Colour figure can be viewed at wileyonlinelibrary.com]

sex differences (Group × Concentration, $P = 0.447$) with a goodness of fit comparison of $R^2 = 0.7861$ for the two data sets (Fig. 1*B*). To further test the vasoactivity of IL-33, *in vivo* mesenteric arterioles (100 ± 5 μm) were assessed by intravital microscopy. Increasing concentrations of IL-33 were delivered by perfusion pump, which produced a significant reduction in intraluminal diameter, –2.38 ± 1.5 μm at 0.1 ng mL^{-1}, −10.76 ± 5.0 μm at 1 ng mL^{-1} and −17.95 ± 6.5 μm at 10 ng mL^{-1} (Fig. 1*C*). These experiments demonstrate that IL-33 increases vascular tone in resistance feed arteries of both sexes.

Mechanism of IL-33-induced vascular tone

To test potential mechanisms of IL-33 action, we first used isolated feed arteries and passed an embolus of air through the vessel lumen, stunning the endothelium and removing its influence on tone. The effectiveness of the air embolus was confirmed by the lack of response 1 μM ACh (% dilatation was significantly reduced from control and not significantly different from). Next, an IL-33 concentration response was conducted, which was not significantly different from control, suggesting IL-33 was acting on the vascular smooth muscle (Group × Concentration $P = 0.705$) (Fig. 2*A*). Therefore, we cultured RASMCs and exposed them to 1 ng mL^{-1} IL-33. We tested whether IL-33 directly induced phosphorylation of the MLC as described previously (Bowdridge et al., 2022) with an in-cell western assay. Stimulation with 1 ng mL^{-1} caused no change in the levels of phosphorylated-MLC ($P = 0.395$) (Fig. 2*B*). To substantiate this finding, we probed for the phosphorylation of ROCK2, CaMK2 and MLC by a traditional western blot. We found no change in activation of these vasoconstriction mediators ($P = 0.228$, $P = 0.413$, $P = 0.274$) (Fig. 2*C*–*E*). However, 1 ng mL^{-1} IL-33 rapidly induced activation of ERK1/2 measured in RASMC at 10 min ($P = 0.0630$) (Fig. 2*F*). Because ERK1/2 is implicated in sensitizing actin-myosin complexes to Ca^{2+}, in VSMC (Kim et al., 2013; Liu & Khalil, 2018), we isolated mesenteric second order feed arteries as before and inhibited ERK1/2 with 5 μM FR180204 for 30 min prior to IL-33 treatment. ERK1/2 inhibition (5 μM FR180204) prevented the IL-33-induced increase in feed artery tone ($P < 0.05$) (Fig. 2*G*). These results demonstrate that IL-33 acts on VSMC in a MyD88 and ERK1/2-dependent manner to increase tone.

IL-33 effect on $Ca^{2\pm}$-mediated responses in isolated feed arteries

To functionally test IL-33-mediated Ca^{2+} sensitization, we examined the responses to myogenic and adrenergic stimulation (PE), which rely on Ca^{2+}-mediated signalling to induce vasoconstriction. Lumen diameter measurements of isolated second order mesenteric feed arteries were taken at intraluminal pressures in the range 20–120 mmHg before and after treatment with 1 ng mL^{-1} IL-33. The presence of 1 ng mL^{-1} IL-33 significantly diminished the diameters at 100 and 120 mmHg ($P < 0.001$ each) (Fig. 3*A*). Similarly, when the myogenic index was calculated, 1 ng mL^{-1} IL-33 had a significant effect at 80 and 100 mmHg (0.26 ± 0.05 *vs.* 0.43 ± 0.04, $P = 0.00480$; –0.05 ± 0.03 *vs.* 0.11 ± 0.02, $P = 0.0104$) (Fig. 3*B*). Finally, the vasoconstriction response to PE was greatly increased in the presence of 1 ng mL^{-1} IL-33 at 100 nM and 1 μM PE (77 ± 3% *vs.* 92 ± 4%, $P = 0.0298$; 56 ± 6% *vs.* 80 ± 7%, $P = 0.0100$) (Fig. 3*C*). Altogether, it is suggested that IL-33 sensitizes feed arteries to stretch and adrenergic stimuli (Ca^{2+}-dependent) causing a greater reduction in vessel diameter and subsequently reduced downstream blood flow.

IL-33 effect on endothelium-dependent dilatation

To test the effect of IL-33 on endothelial function, we isolated second order mesenteric feed arteries (Table 1) and aortic rings for pressure and pin myography, respectively. Feed arteries were subjected to ACh-mediated EDD and then incubated for 1 h with 1 ng mL^{-1} IL-33 to undergo ACh concentration-response again. IL-33 significantly reduced EDD of pressurized mesenteric feed arteries in response to 100 nM and 1 μM ACh compared to control condition (5 ± 1% *vs.* 33 ± 7% and 15 ± 2% *vs.* 50 ± 9%, $P < 0.001$) (Fig. 4*A*). A similar effect was observed via pin myography in aortic rings (Fig. 4*A*). No difference was seen in response to SNP (61 ± 8% *vs.* 56 ± 6%). Because the production of oxidants is known to impact vasoreactivity and the activation of ERK1/2, we assessed both H_2O_2 and $O_2^{\bullet-}$ production. However, 10 ng mL^{-1} IL-33 had no impact on $O_2^{\bullet-}$ production measured by cytochrome C ($P = 0.123$) (Fig. 4*C*), nor H_2O_2 measured by a CBA assay ($P = 0.332$) (Fig. 4*B*). The EPR spin CMH was used to support the cytochrome *c* results. However, CMH showed a statistically significant increase in $O_2^{\bullet-}$ in HAEC treated with IL-33 ($P = 0.0361$) (Fig. 4*C*). This was only a ∼10% increase and potentially because of the promiscuity of the probe. To clarify these findings, we measured peroxynitrite production to determine whether $O_2^{\bullet-}$ was quenching NO and found do difference ($P = 0.1797$) (Fig. 4*C*). Altogether, it is suggested that IL-33-induced EDD impairment is not operant through $O_2^{\bullet-}$ scavenging of NO. In cultured HAEC treated with 10 ng mL^{-1} IL-33 between 0 and 30 min, we observed a rapid and significant activation of ERK1/2, just as in VSMC, with 10 and 15 min producing a more than five-fold increase in the phospho/total ratio compared to time point 0 ($P = 0.0496$ and $P = 0.0078$)

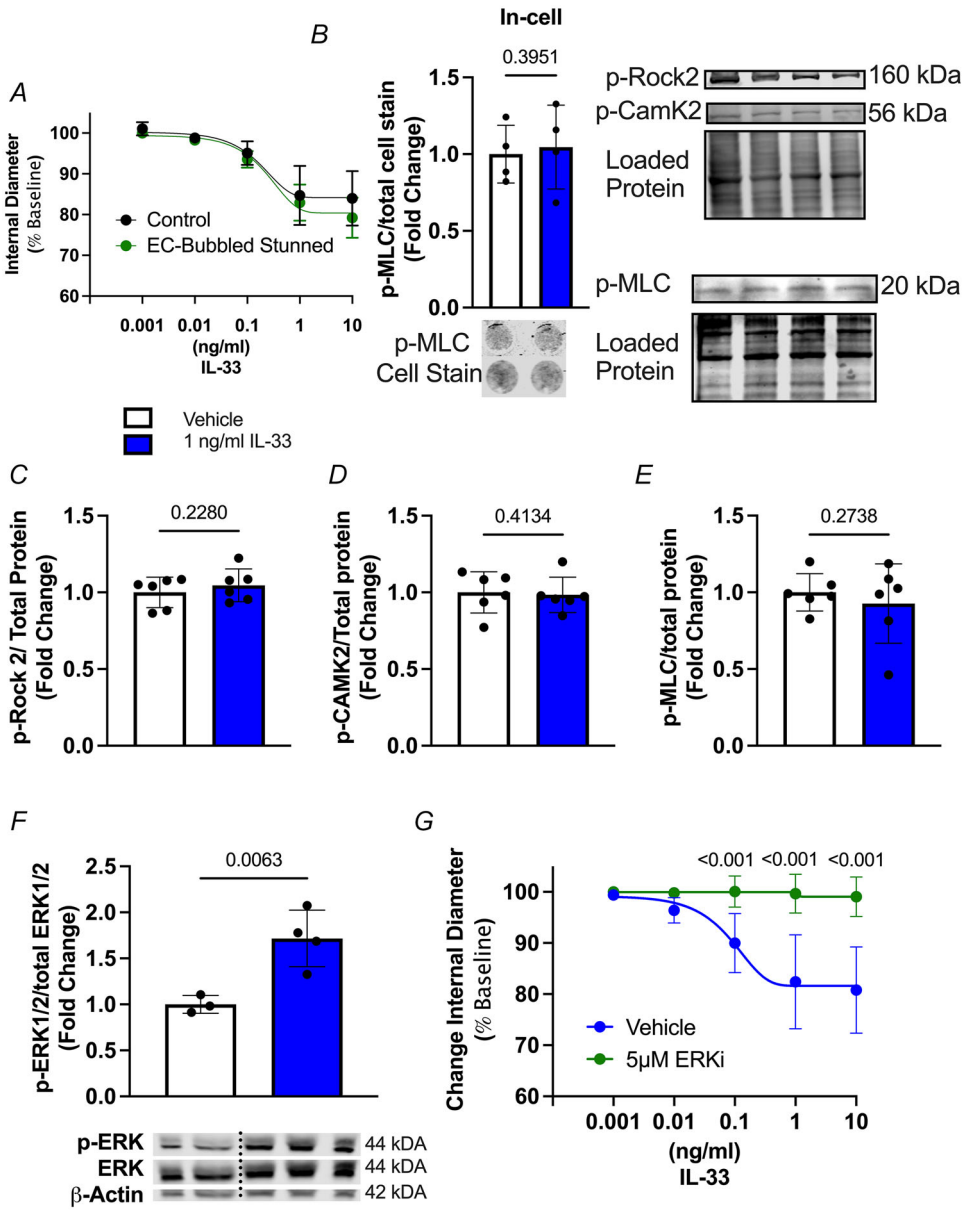

Figure 2. ERK inhibition blocks IL-33-induced vascular tone
A, pressurized second order mesenteric feed-arteries subjected to IL-33 response curve and then an air embolus passed through the lumen to remove endothelial influence and the IL-33 response repeated ($N = 4$, $n = 4$ or 5). Two-way repeated measures ANOVA showed no difference in response (Group × Concentration, $P = 0.705$). *B*, in-cell western for phosphorylated-MLC following IL-33 treatment in RASMC ($n = 4$) analysed by a *t* test $P = 0.395$. *C–E*, traditional western ($n = 6$) blot for phosphorylated-ROCK2, phosphorylated-CaMK2 and phosphorylated-MLC in IL-33-treated *vs.* vehicle-treated RASMC. Analysed by *t* test, $P = 0.228$, $P = 0.413$ and $P = 0.274$, respectively. *F*, Western blot for phosphorylated ERK1/2 in RASMC following IL-33 treatment ($n = 3$ or 4). Analysed by *t* test, $P = 0.0630$. *G*, pressurized mesenteric feed arteries from Sprague–Dawley rats exposed to an increasing concentration of IL-33 ± ERK inhibitor FR180204 ($N = 4$, $n = 6$). Two-way repeated measures ANOVA (Group × Concentration, $P < 0.001$) with Holm–Sidak *post hoc* analysis, which shows $P < 0.001$ at IL-33 concentrations of 0.1, 1 and 10 ng mL^{-1}. Data are the mean ± SD; individual data points and full statistical analysis can be found in the Supplemental data. ERKi, ERK inhibitor. [Colour figure can be viewed at wileyonlinelibrary.com]

(Fig. 4*D*). Although we found no definitive increase in EC oxidant production, we did observe a reduction in NO production, as measured by nitrite/ nitrate reduction with a SEIVERS NO analyser. HAEC treated with 10 ng mL^{-1} IL-33 showed significantly reduced NO production compared to control ($P = 0.00850$) (Fig. 4*E*), which was prevented by ERK1/2 inhibition (5 μM FR180204) ($P = 0.0204$) (Fig. 4*E*). We then interrogated the potential for inhibitory phosphorylation of eNOS by ERK1/2. Serine 602 on eNOS has been reported to be targeted by ERK1/2 causing inhibition. S602 phosphorylation probed following IL-33 treatment showed a two-fold increase ($P = 0.0114$) (Fig. 4*F*), which was completely blocked by ERK1/2 inhibition (5 μM FR180204) ($P = 0.0010$) (Fig. 4*F*). Altogether, it is suggested that IL-33 is acting through ERK1/2 to impair eNOS activity and oppose EDD.

IL-33-ERK1/2 signalling effects in feed arteries of nano-TiO_2 inhalation exposed rats

Our previous study (Abukabda et al. 2018) showed nAb against IL-33 partially prevented nano-TiO_2-induced impairments in EDD. To address whether an IL-33-ERK-S602 eNOS pathway played a role in this, we exposed rats to sham-control (filtered air) or 12 mg m^{-3} nano-TiO_2 on 3 non-consecutive days (Fig. 5*A*). Nano-TiO_2 aerosol size distribution was characterized by SMPS with a median size of 118 nm and geometric SD of 2.09 (Fig. 5*B*). We then isolated

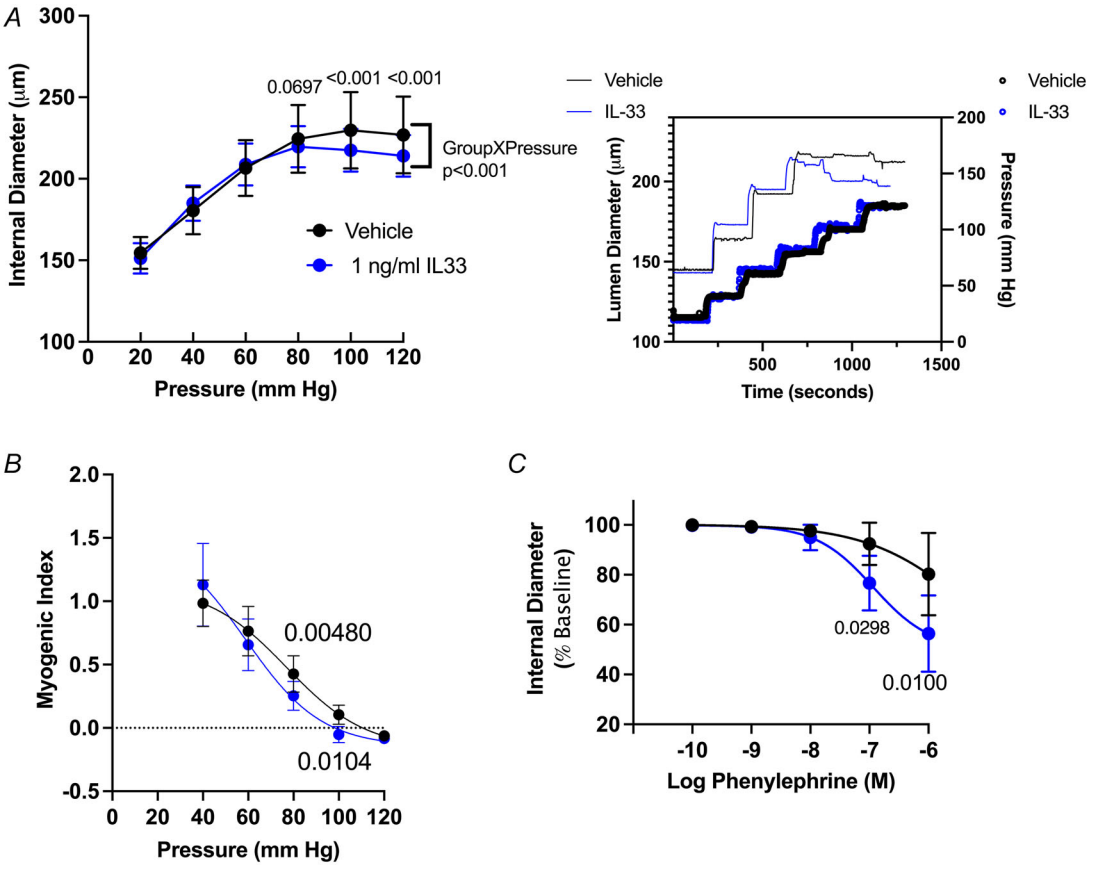

Figure 3. IL-33 augments Ca^{2+}-mediated responses
A, pressurized second order mesenteric feed-arteries from Sprague–Dawley rats ($N = 8$, $n = 13$) incubated ± IL-33 underwent increasing intralumenal pressures to assess the myogenic response with representative pressure diameter tracing. Two-way repeated measures ANOVA (Group × Pressure, $P < 0.001$) with Holm–Sidak *post hoc* analysis, which shows $P < 0.001$ at 100 and 120 mmHg. *B*, the myogenic index was then calculated from this response. Two-way repeated measures ANOVA (Group × Pressure, $P = 0.00190$) with Holm–Sidak *post hoc* analysis, which shows $P = 0.00480$ at 80 mmHg and $P = 0.0104$ at 100 mmHg. *C*, pressurized second order mesenteric feed-arteries from Sprague–Dawley rats incubated ± IL-33 treated with increasing concentrations of phenylephrine ($N = 4$, $n = 6$). Two-way repeated measures ANOVA (Group × Pressure, $P = 0.00670$) with Holm–Sidak *post hoc* analysis, which shows $P = 0.0298$ at 100 nM phenylephrine and $P = 0.0100$ at 1 μM phenylephrine. Data are the mean ± SD; individual data points and full statistical analysis can be found in the Supplemental data. [Colour figure can be viewed at wileyonlinelibrary.com]

feed arteries from sham and nano-TiO_2 rats (Table 2) and performed ACh-mediated EDD experiments ± ERK1/2 inhibitor (5 μM FR180204) and reperformed the ACh-EDD experiment. As before (Abukabda et al., 2018), nano-TiO_2 inhalation exposure caused a significant impairment to ACh-mediated EDD (Fig. 5*C*), which was partially recovered by ERK1/2 inhibition (5 μM FR180204) (Fig. 5*C*). We further tested whether the IL-33-mediated increase in feed artery tone was altered following nano-TiO_2 exposure. IL-33-induced increases in vascular tone were observed in both sham-controls and nano-TiO_2 exposed mesenteries, with the inhalation

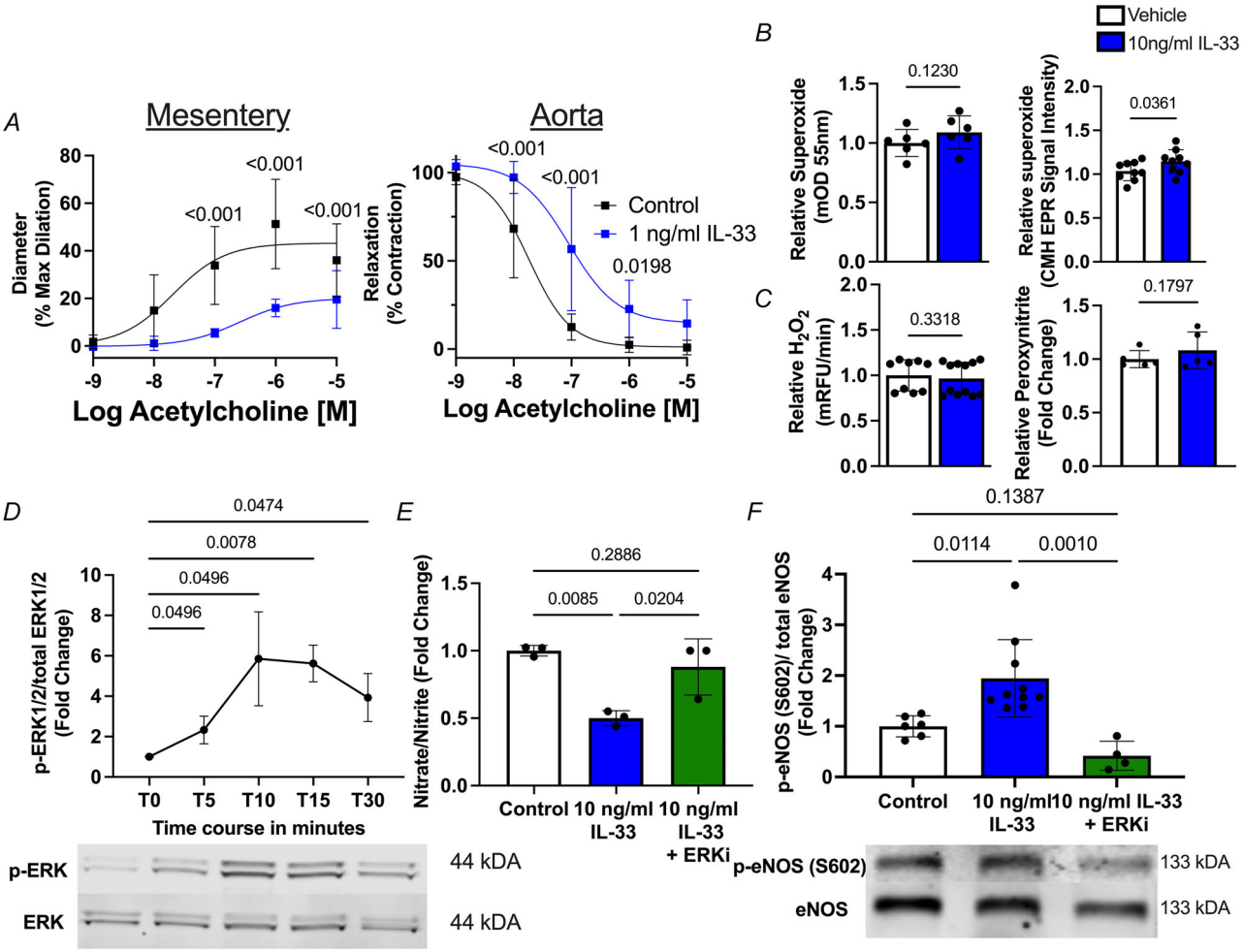

Figure 4. IL-33 opposes nitric oxide and endothelial-dependent dilatation
A, pressurized second order mesenteric feed-arteries and pin mounted aortic rings from Sprague–Dawley rats incubated ± IL-33 were exposed to increasing concentrations of ACh to assess EDD ($N = 5$ and 6, $n = 5$–7). Two-way repeated measures ANOVA (Group × Concentration, $P < 0.001$) for both the mesentery and the aorta. Holm–Sidak *post hoc* analysis, which shows $P < 0.001$ at 100 nM, 1 μM and 10 μM ACh in the mesentery and $P < 0.001$ at 10 nM and 100 nM and $P = 0.0198$ at 1 μM ACh in the aorta. *B* and *C*, cultured HAEC-treated ± IL-33 and superoxide production measured cytochrome c (*t* test, $P = 0.123$) and EPR (*t* test, $P = 0.0361$) ($n = 6$–9) or hydrogen peroxide measured by a CBA assay (*t* test, $P = 0.3318$) ($n = 9$–12). *D*, HAEC-treated ± IL-33 for 0–30 min and phospho/total ratio of ERK1/2 measured by western blot ($n = 4$). Analysed by one-way repeated measures ANOVA with Holm–Sidak *post hoc* analysis compared to T0. T5 *vs*. T0, $P = 0.0496$; T10 *vs*. T0, $P = 0.0496$; T15 *vs*. T0, $P = 0.00780$; and T30 *vs*. T0, $P = 0.0474$. *E*, HAEC treated with IL-33 ± ERK inhibition with FR180204 and stimulated by A23187. Then, media were collected and NO production was measured via nitrate/nitrite reduction ($n = 3$, each measured in triplicate). Analysed by one-way ANOVA with Holm–Sidak *post hoc* analysis: IL-33 *vs*. vehicle control, $P = 0.00850$; IL-33 *vs*. IL-33 + ERKi, $P = 0.0204$; and IL-33 + Erki *vs*. vehicle control, $P = 0.289$. *F*, finally, phospho/total ratio of serine 602 of eNOS was measured by western blot ($n = 4$–10). Analysed by one-way ANOVA with Holm–Sidak *post hoc* analysis: IL-33 *vs*. vehicle control, $P = 0.0114$; IL-33 *vs*. IL-33 + ERKi, $P = 0.00100$; and IL-33 + Erki *vs*. vehicle control, $P = 0.139$. Data are the mean ± SD; individual data points and full statistical analysis can be found in the Supplemental data. ERKi, ERK inhibitor. [Colour figure can be viewed at wileyonlinelibrary.com]

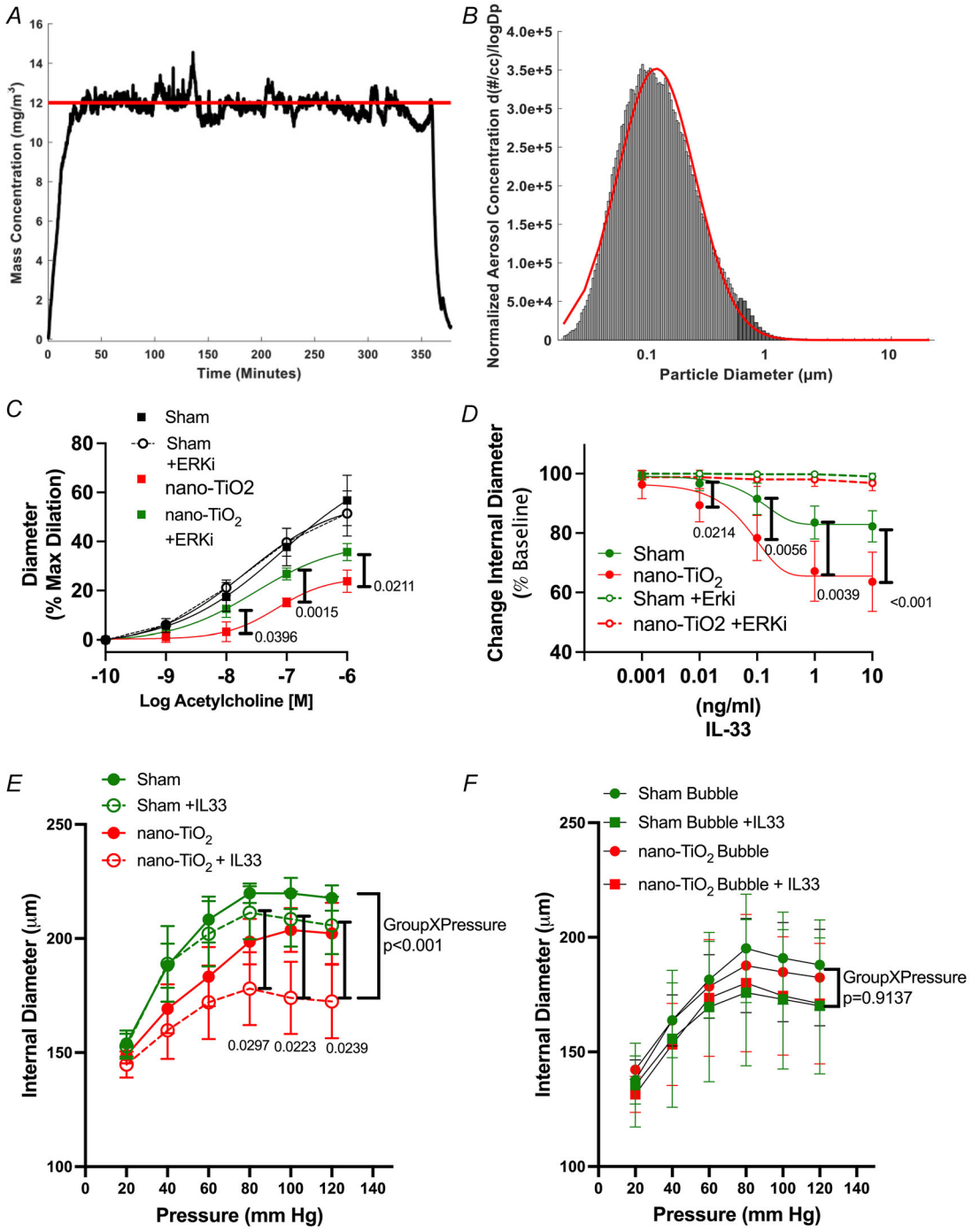

Figure 5. Vascular responses, nano-TiO_2 inhalation exposed rats
A, representative real-time mass concentration measurement of aerosolized nano-TiO_2 during an exposure the red-line indicates the target concentration of 12 mg m^{-3}. *B*, particle size distribution of nano-TiO_2 aerosol (mobility diameter) samples directly from the exposure chamber using a scanning mobility particle sizer (SMPS, light grey) and an aerodynamic particle sizer (APS, dark grey) The red line indicates the log-normal fit of the histogram (count median diameter 118 nm and geometric SD of 2.09). *C* and *D*, EDD and IL-33 response ± ERK inhibition with FR180204 measured in pressurized second order mesenteric feed-arteries from sham and nano-TiO_2 inhalation exposed rats (N = 4–6, n = 4–10). Two-way repeated measures ANOVA (Group × Concentration, $P < 0.001$) with Holm–Sidak *post hoc* analysis: nano-TiO_2 *vs.* nano-TiO_2 + ERKi indicates $P = 0.0396$ at 100 nM ACh, $P = 0.00150$ at 1 µM ACh and $P = 0.0211$ at 10 µM ACh. Two-way repeated measures ANOVA of the IL-33 response (Group × Concentration, $P < 0.001$) Holm–Sidak *post hoc* analysis: sham *vs.* nano-TiO_2 shown at IL-33 concentrations of 0.01 ng mL^{-1} ($P = 0.0214$), 0.1 ng mL^{-1} ($P = 0.00560$), 1 ng mL^{-1} ($P = 0.00390$) and

10 ng mL^{-1} ($P < 0.001$). *E*, pressurized second order mesenteric feed-arteries from Sprague–Dawley rats ($N = 4$ or 5, $n = 4$ or 5) incubated ± IL-33 were subjected to intralumenal pressures between 20 and 120 mmHg to determine the myogenic response. Two-way repeated measures ANOVA (Group × Pressure, $P < 0.001$) Holm–Sidak *post hoc* analysis: sham + IL-33 *vs*. nano-TiO_2 + IL-33 shown at 80 mmHg ($P = 0.0297$), 100 mmHg ($P = 0.0223$) and 120 mmHg ($P = 0.0239$). *F*, these differences were not seen in bubble stunned second order mesenteric feed-arteries. Two-way repeated measures ANOVA ($P = 0.914$) ($N = 4$ or 5, $n = 4$ or 5). Data are the mean ± SD; individual data points and full statistical analysis can be found in the Supplemental data. ERKi, ERK inhibitor. [Colour figure can be viewed at wileyonlinelibrary.com]

Table 2. Mesentery feed-artery characteristics from exposed and sham male and female rats

	N (*n*)	Lumen diameter @ 70 mmHg (μm)	Outer diameter @ 70 mmHg (μm)	% Vascular tone
Sham	7 (15)	218.4 ± 24.6	260.5 ± 27.4	24.1 ± 2.1
Nano-TiO_2	7 (9)	204.1 ± 17.9	249.0 ± 19.6	25.6 ± 3.5
Statistical comparison		$P = 0.131$	$P = 0.250$	$P = 0.154$

Data is represented as the mean ± SD. Statistical comparison between groups was conducted by a *t* test. *N* is the number of rats and *n* is the number of vessels.

exposed feed arteries demonstrating augmented increases in tone at 0.01 ng mL^{-1} IL-33 ($P = 0.0214$), 0.1 ng mL^{-1} IL-33 ($P = 0.0056$), 1 ng mL^{-1} IL-33 ($P = 0.0039$) and 10 ng mL^{-1} IL-33 ($P < 0.001$) compared to the sham-controls (Fig. 5*D*). The IL-33 response was once again blocked by ERK1/2 inhibition (5 μM FR180204) (Fig. 5*D*) Likewise, air embolism-induced stunning of the endothelium had no effect on either sham-control or nano-TiO_2 feed arteries response to IL-33. Next the myogenic response was tested in sham and nano-TiO_2 feed arteries with and without an air embolus and ±1 ng mL^{-1} of IL-33. With intact endothelium, the nano-TiO_2 feed arteries demonstrated an augmented myogenic response when incubated with IL-33 (Group × Concentration $P < 0.001$) (Fig. 5*E*) and highlighted a significant difference in feed artery diameter at 80 mmHg ($P = 0.0297$), 100 mmHg ($P = 0.0223$) and 120 mmHg ($P = 0.0239$) between sham + IL-33 and nano-TiO_2 + IL-33. After stunning the endothelium with an air embolus, the internal diameter dropped at each pressure compared to intact endothelium and IL-33 further reduced the normalized diameter. However, the air embolus eliminated the difference between sham-control and nano-TiO_2 (Fig. 5*F*). Altogether, it is suggested that IL-33-ERK plays a role in ENM-induced vascular impairment and that vessels from ENM exposed animals have an augmented responses to IL-33.

Ruptured endothelial cells cause increased vascular tone in part through IL-33

In addition to IL-33 released during toxicant inhalation, acutely damaged endothelial cells also have the potential to release IL-33 at the site of vascular injury. First, we confirmed that human IL-33 acted on isolated rat feed arteries. As such, we collected cultured HAEC media from control and mechanically ruptured EC and added increasing volumes into the pressure myography bath. Culture media was added to isolated second order mesentery feed arteries at the indicated volumes ± pretreatment with 100 nM IL-33 nAb. Ruptured HAEC media caused a significant reduction in internal diameter at 5, 10, 50 and 100 μL of added media compared to control media ($P < 0.001$) (Fig. 6). The treatment of ruptured HAEC conditioned media with IL-33 nAb prior to the addition partially prevented the decrease in second order mesentery feed arteries internal diameter compared to

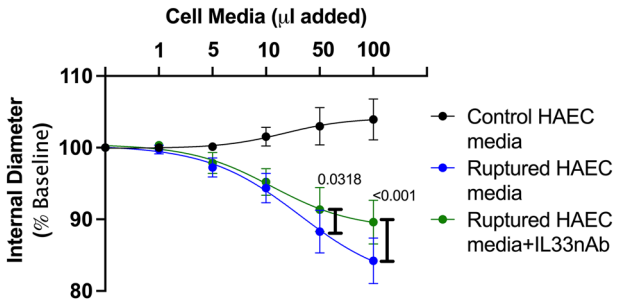

Figure 6. Mechanically ruptured endothelial cells cause increased feed artery tone in part via IL-33
Pressurized second order mesenteric feed-arteries from Sprague–Dawley rats were exposed to increasing volumes of HAEC cell conditioned media ± pretreatment with IL-33 nAb. ($N = 6$, $n = 9$–11). Two-way repeated measures ANOVA (Group × Concentration, $P < 0.001$) Holm–Sidak *post hoc* analysis: $P < 0.001$ control *vs*. ruptured at 5, 10, 50 and 100 μL. Furthermore, Holm–Sidak *post hoc* analysis indicated a significant difference between ruptured media and ruptured media + IL-33 nAb at 50 μL, $P = 0.0318$ and 100 μl, $P < 0.001$. Data are the mean ± SD; individual data points and full statistical analysis can be found in the Supplemental data. [Colour figure can be viewed at wileyonlinelibrary.com]

ruptured HAEC media, reaching significance at 50 and 100 µL of added media ($P = 0.0318$ and $P < 0.001$) (Fig 6). Altogether, it is suggested IL-33 may serve to augment vascular tone upon vascular injury.

IL-33 requires ST2 to cause ERK phosphorylation

As a result of our inability to directly target ST2 in our isolated vessel experiments, we tested whether ST2 was required for ERK activation in our HAECs because commercially available ST2 nAB only target the human receptor. Using HAEC we pretreated with 0.8 µg mL^{-1} ST2 nAB (0.1 µg mL^{-1} is the IC_{50} for 1 ng mL^{-1} IL-33) and then treated with 1 ng mL^{-1} IL-33. The pretreatment of HAEC with ST2 nAB blocked the IL-33 activation of ERK 1/2 ($P = 0.0108$ IL-33 *vs.* IL-33 + ST2nAB) (Fig. 7).

Discussion

The data reported in the present study reveal a novel action of the alarmin IL-33 on arterial tone and endothelial-mediated dilatation via ERK1/2 activation. By means of pressurized arteries, we demonstrate that IL-33 induces a concentration-dependent decrease in lumen diameter and augments Ca^{2+}-mediated responses to myogenic and adrenergic stimuli, which is dependent on MyD88 and ERK1/2 (Figs 1–3). Furthermore, incubation of feed arteries with 1 ng mL^{-1} IL-33 diminishes the dilatory response to ACh. IL-33 treatment of cultured EC revealed inhibitory phosphorylation of eNOS and mitigated NO production. Mechanistically, we demonstrate that pharmaceutical inhibition of ERK1/2 in isolated feed arteries and cultured EC abolished the actions of IL-33 (Fig. 4). Finally, to provide more physiological insights into how disruption of barrier cells might influence vascular tone, we explored two known sources of circulating IL-33 (lung damage from toxicant inhalation and EC rupture). Using these approaches, we demonstrate that IL-33-ERK1/2 is a key component of increased vascular tone to reduce blood flow following barrier cell injury.

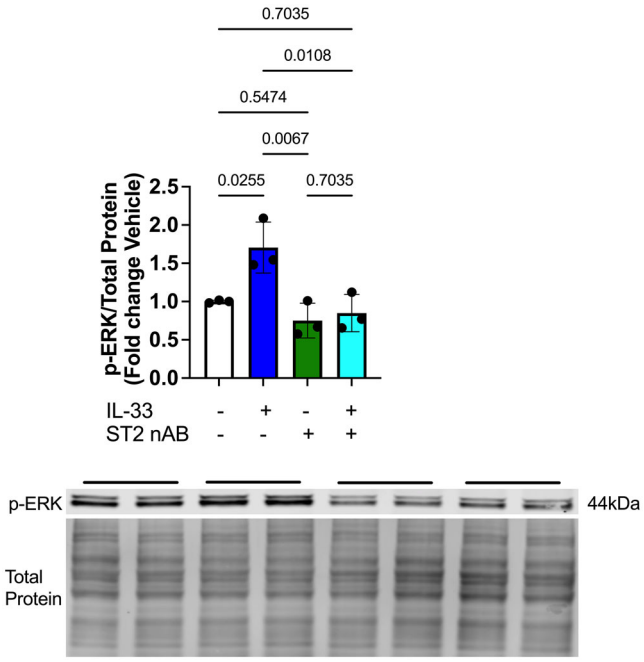

Figure 7. IL-33 requires the ST2 receptor to activate ERK 1/2
Cultured HAEC were pretreated with 0.8 µg/ml of ST2nAB or vehicle control for 30 min and then treated with 1 ng mL^{-1} of IL-33 or vehicle for 10 min collected and ERK1/2 phosphorylation measured by western blot normalized to total protein. One-way ANOVA with Holm–Sidak *post hoc* analysis detected a significant increase in phosphorylated-ERK in IL-33 *vs.* vehicle ($P = 0.0205$), which was prevented by the ST2nAB ($P = 0.0108$). Data are the mean ± SD; individual data points. [Colour figure can be viewed at wileyonlinelibrary.com]

Although a clear role for alarmins in immune and allergic responses has been well established, these mediators are also released into the circulation and the present study focuses on the acute actions of the IL-33 alarmin on the vasculature. The concentration of IL-33 used in the present study falls within previously observed ranges of circulating (10–400 pg mL^{-1}) and local tissue concentrations following allergic responses (>30 ng mg^{-1}) (Gluck et al., 2012; Iijima et al., 2014; Ozturan et al., 2017). Our previous work, at an acute time point, suggested that IL-33 may be involved in vascular dysfunction following lung exposure to ENM. In that study, administration of an IL-33 nAb preserved EDD following ENM inhalation exposure (Abukabda et al., 2018). Importantly, this same study demonstrated both elevated lung and circulating levels of IL-33 (Abukabda et al., 2018) following ENM exposure. However, it was unclear from these experiments whether IL-33 blockade was having affects directly on the vasculature or whether these were secondary to blockade of lung inflammation. In the present study, we demonstrate that IL-33 acts directly on the vasculature and induces a concentration-dependent reduction in lumen diameter of mesenteric second order feed arteries, both isolated and *in vivo*. This is in line with the actions of other alarmins that acutely promote increased vascular tone (Bhagat & Vallance, 1997; Cavalli et al., 2021; Kauffenstein et al., 2010; Zhu et al., 2020). Conversely, IL-33 had no impact on baseline tension of conduit arteries mounted in a pin myography prep (unpublished observation, DeVallance & Nurkiewicz (ED&TRN)). Altogether, it is suggested that IL-33-induced increases in vascular tone may involve pathways that do not directly result in increased free Ca^{2+}.

With the knowledge that IL-33 was acting to increase arterial tone, we proceeded to determine whether this was through direct action on the VSMC. Using an air

embolus, we removed the influence of the endothelium on vascular tone to illustrate that IL-33 was acting on the VSMC (Fig. 2*A*). Unlike 'traditional' vasoconstrictors (PE, angiotensin II, endothelin-1) (Abe et al., 1991; Annibale et al., 1990; Benze et al., 1991), IL-33 did not increase MLC phosphorylation, nor the activation of upstream mediators, which aligns with our observation that IL-33 did not alter baseline tension of aortic rings in pin myography experiments. This suggested that IL-33 was probably not acting to mobilize Ca^{2+}, but rather was working through an alternative pathway. Canonical IL-33 signalling pathways involve the ST2 receptor, its adaptor MyD88 and mitogen-activated protein kinases (Griesenauer et al., 2019; Pan et al., 2019), which can influence vasoconstriction in the absence of MLC phosphorylation (Jiang & Morgan, 1989). Mitogen-activated protein kinases and specifically ERK1/2 can interact with/regulate calponin and caldesmon activity, which serves to sensitize the contractile proteins in VSMC to Ca^{2+}, thus augmenting vasoconstriction at a given Ca^{2+} load (Childs & Mak, 1993; Huang et al., 2003; Je et al., 2001; Leinweber et al., 1999; Liu & Khalil, 2018; EL-Mezgueldi & Marston, 1996; Patchell et al., 2002; Winder & Walsh, 1993; Winder et al., 1993). In the present study, direct antagonism of the ST2 receptor in isolated vessels was not possible because these compounds are only in the computational phase of development, but our data show that the IL-33 response in isolated pressurized feed arteries is dependent on both MyD88 and ERK1/2, suggesting a canonical signalling pathway. Subsequently, the ERK1/2 activation augments Ca^{2+}-mediated responses (Baek & Kim, 2011; Lee et al., 2001). Physiologically, this suggests that IL-33 may prime vessels to hyper-respond to sympathetic and myogenic inputs. Augmenting these responses would further reduce downstream blood flow and enhance the surface to blood volume ratio to enhance clotting efficiency and immune cell interaction in response to cellular damage (Rodrigues et al., 2019). Thus, IL-33 released in areas of cellular damage may serve to fine tune local blood flow, which serves to aid initiation of wound healing.

Although IL-33 regulation of feed artery tone did not require the endothelium, proceeding on past observations, we demonstrate another novel action of IL-33 acting on the endothelium to oppose ACh-EDD. Our initial speculation was that IL-33 initiated the production of $O_2^{\bullet -}$. However, we detected no difference in $O_2^{\bullet -}$ or H_2O_2 when treating HAEC with 10 ng mL^{-1} IL-33. Although the results in our EPR experiment were statistically significant, it was only a 10% increase in oxidant production, which made us question the physiological relevance. To clear up the potential role for oxidant-induced reduction of NO, we measured peroxynitrite formation (product of $O_2^{\bullet -}$ scavenged NO), but again found no significant difference. Altogether, because we observed this meager increase in oxidant production in only one of four assays when treating with our maximum concentration of IL-33 (10 ng mL^{-1}), we are skeptical that it has a major physiological implication. However, we cannot completely rule out its minor involvement at high concentrations of IL-33. Regardless, IL-33 induces ERK1/2 phosphorylation in the endothelium dependent on the ST2 receptor, as in VSCM, confirming activation of its canonical signalling pathway. It was interesting to find a previous report from Salerno et al. (2014) suggesting ERK1/2 inhibition of eNOS. We then postulated IL-33 activation of ERK1/2-mediated eNOS inhibition as a mechanism for IL-33 reduction of EDD. Indeed, our treatment of HAEC with IL-33 $\pm$ ERK inhibition (Fig. 4) supports the idea that this pathway is operative and opposes eNOS-NO regulation of vascular tone. In a greater context, these findings align with many known and speculated actions of other alarmins [HMGB1 (Zhu et al., 2020), uric acid (Park et al., 2013), IL-1a (Bhagat & Vallance, 1997; Cavalli et al., 2021) and TLR-4 targeted molecules (Yazji et al., 2013; Zhu et al., 2020)], which demonstrate similar impairment of EDD through eNOS-dependent mechanisms. However, ATP is a notable exception that has both vasodilatory and vasoconstrictive properties depending on the concentration and rate of metabolism (Eroglu et al., 2019; Kauffenstein et al., 2010; Lohman et al., 2012). Altogether, this suggests a conserved functional role of most alarmins to locally increase vascular tone and oppose EDD.

Our evidence thus far has demonstrated that recombinant IL-33 regulated feed artery function. *In vivo*, IL-33 can be processed and released similar to other IL-1 family members following injury, as in ENM-inhalation induced injury (Lefrancais & Cayrol, 2012; Lefrancais et al., 2014; Lefrancais et al., 2012; Roussel et al., 2008; Travers et al., 2018). However, unlike other family-members, the full-length unprocessed IL-33 is also active and could act as an alarmin from ruptured cells in vascular injury (Cayrol & Girard, 2009; Ferhat et al., 2018; Luthi et al., 2009; Talabot-Ayer et al., 2009). Based on this knowledge, we examined whether ENM-inhalation induced vascular impairment (Abukabda et al., 2018) involved IL-33-ERK and whether IL-33 released from mechanically ruptured EC increased vascular tone. Our results demonstrate a role for ERK1/2-induced opposition of EDD following ENM inhalation exposure. Additionally, we found that feed arteries following ENM inhalation exposure demonstrate an augmented response to IL-33. We speculate this is a result of the documented EC impairment and increased resting tone observed in ENM inhalation exposed animals, which is augmented by IL-33 treatment (Nurkiewicz et al., 2004, 2008, 2009). This idea is supported by our data showing air embolus normalizes the IL-33 response (Fig. 5*F*). Moving to our *in*

vitro model of vascular injury, we show ruptured HAEC (mechanical scraping) conditioned media increases vascular tone, which is in part dependent on IL-33. Altogether, these findings suggest that IL-33 contributes to vascular function and blood flow regulation following barrier cell damage.

In the context of the greater literature on IL-33 in cardiovascular function, our results at first seem at odds with the previous findings. However, these actions of IL-33 again align with other alarmins such as HMGB1 and IL-1 that not only increase vascular tone, but also promote angiogenesis and immune cell recruitment (Kindle et al., 2006; Lan et al., 2020; Salmeron et al., 2016). It is plausible the acute actions of IL-33 on EC and VSMC detailed in the present study promote the documented long-term cardioprotective functions of IL-33 (Choi et al., 2009; Ghali et al., 2018; Pentz et al., 2018; Sanada et al., 2007; Turnquist et al., 2011). Worthy of note, a recent study has shown IL-33 signalling to be involved in kidney-induced cardiomyopathy (Florens et al., 2023). However, this appears to be through actions on the heart and not the vasculature. Specific to the well documented IL-33-induced EC proliferation, increased vascular tone (shown in Fig. 1) and thus a stiffer extracellular matrix may serve to promote EC proliferation (LaValley et al., 2017; Yeh et al., 2012). Additionally, ERK promotes proliferation (Song et al., 2023), as well as eNOS inhibition (Salerno et al., 2014) and, somewhat counterintuitively, small interfering RNA knockdown of eNOS has been shown to increase EC proliferation and migration (Bu et al., 2022). Altogether, there is evidence that IL-33 initially promotes increased tone/reduced blood flow to an area of barrier cell injury; however, these 'acute' actions may serve to promote vascular repair and lend to the documented reports of the cardioprotective effects of IL-33. Defining the transcriptional and epigenomic pathways linking our acute observation in the present study with the long-term cardioprotective effects of IL-33 is of future interest.

Limitations

Although we employed multiple approaches to demonstrate the actions of IL-33 on acute vascular function, the present study is not without limitations. First, the effects of IL-33 on ERK and MLC phosphorylation were tested in cultured RASMC and not VSMC from resistance vessels. As such, subtle physiological difference may exist between these cell types. Furthermore, although RASMC were serum starved to drive a contractile phenotype, there is the possibility that VSMC phenotype differs from that *in vivo* and influenced our findings. However, collectively, our observations that IL-33 did not active MLC, ROCK or CaMK in RASMC did not alter tension in pin myography experiments, but did augment Ca^{2+}-mediated responses and corroborate our interpretation of the results. Second, it is well-known that arteriolar EDD is only partially dependent on eNOS-NO. Although we show significant inhibitory eNOS phosphorylation and diminished NO production in cultured HAEC corresponding with diminished EDD of feed arteries, how the other vasodilatory mediators are impacted by IL-33 and contribute to this reduction in EDD was not interrogated. Third, although we demonstrate no sex differences in Fig. 1*B*, we did not investigate whether this held true following exposure. Both males and females were used in the exposure experiment, but we were not powered to analyse any potential sex differences. However, we can state, germane to the aim of the study, that both male and female vessels respond to IL-33 following exposure. Fourth, we use mesenteric feed arteries to assess myogenic responses. Even smaller mesenteric arterioles do not exhibit textbook myogenic tone seen in cerebral or kidney microvessels (Turner et al., 2019). However, even though these vessels exhibit weak myogenic responses, this intrinsic response to limit lumen diameter or constrict in the presence of increasing intralumenal pressure requires Ca^{2+}. The aim in using this response was to demonstrate that the presence of IL-33 augmented Ca^{2+}-mediated responses, which our data clearly demonstrate and are further supported by Fig. 3*C*. Fifth, because of lack of rat-specific neutralizing antibodies and an inability to use small interfering RNA against ST2 in isolated vessels (time constraint of tissue viability), we had to target downstream effectors in isolated vessel experiments. However, proof-of-concept experiments in Fig. 7 demonstrate *in vitro* that IL-33 requires ST2 to induce ERK phosphorylation in vascular cells. Finally, we do not directly test the activation of Ca^{2+} sensitizing proteins calponin and caldesmon. However, based on these proteins being known targets of ERK, in addition to our observations that IL-33 augments Ca^{2+}-mediated responses without activation of ROCK, CaMK or phosphorylation of MLC along with IL-33 requiring active tone to illicit a response (no effect in pin myography), we speculate their involvement.

Conclusions

In summary, the present study provides novel evidence for alarmin IL-33 mediating vascular function following its release. Our findings demonstrate that IL-33 augments Ca^{2+}-mediated vascular tone dependent on a MyD88-ERK1/2 pathway. Additionally, IL-33 impairs EDD through the ERK1/2-induced inhibition of eNOS. Altogether, the present study defines a novel vasoactive role for the alarmin IL-33 and suggests that it may play

a role in blood flow regulation following barrier cell injury. Future studies will be aimed at understanding the transcriptional/epigenetic pathways involved in linking the acute IL-33 actions observed in the present study with the previously reported chronic cardiovascular protective effects of IL-33.

References

Abe, Y., Kasuya, Y., Kudo, M., Yamashita, K., Goto, K., Masaki, T., & Takuwa, Y. (1991). Endothelin-1-induced phosphorylation of the 20-kDa myosin light chain and caldesmon in porcine coronary artery smooth muscle. *Japanese Journal of Pharmacology*, **57**(3), 431–435.

Abukabda, A. B., Bowdridge, E. C., McBride, C. R., Batchelor, T. P., Goldsmith, W. T., Garner, K. L., Friend, S., & Nurkiewicz, T. R. (2019). Maternal titanium dioxide nanomaterial inhalation exposure compromises placental hemodynamics. *Toxicology and Applied Pharmacology*, **367**, 51–61.

Abukabda, A. B., McBride, C. R., Batchelor, T. P., Goldsmith, W. T., Bowdridge, E. C., Garner, K. L., Friend, S., & Nurkiewicz, T. R. (2018). Group II innate lymphoid cells and microvascular dysfunction from pulmonary titanium dioxide nanoparticle exposure. *Particle and Fibre Toxicology*, **15**(1), 43.

Abukabda, A. B., Stapleton, P. A., McBride, C. R., Yi, J., & Nurkiewicz, T. R. (2017). Heterogeneous vascular bed responses to pulmonary titanium dioxide nanoparticle exposure. *Frontiers in Cardiovascular Medicine*, **4**, 33.

Annibale, D. J., Rosenfeld, C. R., Stull, J. T., & Kamm, K. E. (1990). Protein content and myosin light chain phosphorylation in uterine arteries during pregnancy. *American Journal of Physiology*, **259**(3 Pt 1), C484–C489.

Baek, E. B., & Kim, S. J. (2011). Mechanisms of myogenic response, Ca(2+)-dependent and -independent signaling. *Journal of Smooth Muscle Research*, **47**, 55–65.

Beamer, C. A., Girtsman, T. A., Seaver, B. P., Finsaas, K. J., Migliaccio, C. T., Perry, V. K., Rottman, J. B., Smith, D. E., & Holian, A. (2013). IL-33 mediates multi-walled carbon nanotube (MWCNT)-induced airway hyper-reactivity via the mobilization of innate helper cells in the lung. *Nanotoxicology*, **7**(6), 1070–1081.

Benze, J., Yang, H. Y., Griffith, V. J., & Rosendorff, C. (1991). Angiotensin II induced phosphorylation of myosin light chain in vascular smooth muscle cells from spontaneously hypertensive and normotensive rats. *Cardiovascular Research*, **25**(8), 617–621.

Bhagat, K., & Vallance, P. (1997). Inflammatory cytokines impair endothelium-dependent dilatation in human veins in vivo. *Circulation*, **96**(9), 3042–3047.

Bowdridge, E. C., DeVallance, E., Garner, K. L., Griffith, J. A., Schafner, K., Seaman, M., Engels, K. J., Wix, K., Batchelor, T. P., Goldsmith, W. T., Hussain, S., & Nurkiewicz, T. R. (2022). Nano-titanium dioxide inhalation exposure during gestation drives redox dysregulation and vascular dysfunction across generations. *Particle and Fibre Toxicology*, **19**, 18.

Branyan, K. W., Devallance, E. R., Lemaster, K. A., Skinner, R. C., Bryner, R. W., Olfert, I. M., Kelley, E. E., Frisbee, J. C., & Chantler, P. D. (2018). Role of chronic stress and exercise on microvascular function in metabolic syndrome. *Medicine and Science in Sports and Exercise*, **50**(5), 957–966.

Brooks, S. D., deVallance, E., d'Audiffret, A. C., Frisbee, S. J., Tabone, L. E., Shrader, C. D., Frisbee, J. C., & Chantler, P. D. (2015). Metabolic syndrome impairs reactivity and wall mechanics of cerebral resistance arteries in obese Zucker rats. *American Journal of Physiology-Heart and Circulatory Physiology*, **309**(11), H1846–H1859.

Bu, S., Nguyen, H. C., Nikfarjam, S., Michels, D. C. R., Rasheed, B., Maheshkumar, S., Singh, S., & Singh, K. K. (2022). Endothelial cell-specific loss of eNOS differentially affects endothelial function. *PLoS ONE*, **17**(9), e0274487.

Cavalli, G., Colafrancesco, S., Emmi, G., Imazio, M., Lopalco, G., Maggio, M. C., Sota, J., & Dinarello, C. A. (2021). Interleukin 1alpha, a comprehensive review on the role of IL-1alpha in the pathogenesis and treatment of autoimmune and inflammatory diseases. *Autoimmunity Reviews*, **20**(3), 102763.

Cayrol, C., & Girard, J. P. (2009). The IL-1-like cytokine IL-33 is inactivated after maturation by caspase-1. *Proceedings of the National Academy of Sciences*, **106**(22), 9021–9026.

Cayrol, C., & Girard, J. P. (2014). IL-33, An alarmin cytokine with crucial roles in innate immunity, inflammation and allergy. *Current Opinion in Immunology*, **31**, 31–37.

Childs, T. J., & Mak, A. S. (1993). Smooth-muscle mitogen-activated protein (MAP) kinase, Purification and characterization, and the phosphorylation of caldesmon. *Biochemical Journal*, **296**(Pt 3), 745–751.

Choi, Y. S., Choi, H. J., Min, J. K., Pyun, B. J., Maeng, Y. S., Park, H., Kim, J., Kim, Y. M., & Kwon, Y. G. (2009). Interleukin-33 induces angiogenesis and vascular permeability through ST2/TRAF6-mediated endothelial nitric oxide production. *Blood*, **114**(14), 3117–3126.

de Jesus, D. S., de Vallance, E., Li, Y., Falabella, M., Guimaraes, D., Shiva, S., Kaufman, B. A., Gladwin, M. T., & Pagano, P. J. (2019). Nox1/Ref-1-mediated activation of CREB promotes Gremlin1-driven endothelial cell proliferation and migration. *Redox Biology*, **22**, 101138.

Deiana, C., Minella, M., Tabacchi, G., Maurino, V., Fois, E., & Martra, G. (2013). Shape-controlled TiO2 nanoparticles and TiO2 P25 interacting with CO and H2O2 molecular probes, a synergic approach for surface structure recognition and physico-chemical understanding. *Physical Chemistry Chemical Physics*, **15**(1), 307–315.

DeVallance, E., Branyan, K. W., Lemaster, K. C., Anderson, R., Marshall, K. L., Olfert, I. M., Smith, D. M., Kelley, E. E., Bryner, R. W., Frisbee, J. C., & Chantler, P. D. (2019). Exercise training prevents the perivascular adipose tissue-induced aortic dysfunction with metabolic syndrome. *Redox Biology*, **26**, 101285.

DeVallance, E. R., Dustin, C. M., de Jesus, D. S., Ghouleh, I. A., Sembrat, J. C., Cifuentes-Pagano, E., & Pagano, P. J. (2022). Specificity protein 1-mediated promotion of CXCL12 advances endothelial cell metabolism and proliferation in pulmonary hypertension. *Antioxidants (Basel)*, **12**(1), 71.

EL-Mezgueldi, M., & Marston, S. B. (1996). The effects of smooth muscle calponin on the strong and weak myosin binding sites of F-actin. *Journal of Biological Chemistry*, **271**(45), 28161–28167.

Eroglu, E., Saravi, S. S. S., Sorrentino, A., Steinhorn, B., & Michel, T. (2019). Discordance between eNOS phosphorylation and activation revealed by multispectral imaging and chemogenetic methods. *Proceedings National Academy of Science USA*, **116**, 20210–20217.

Ferhat, M., Robin, A., Giraud, S., Sena, S., Goujon, J. M., Touchard, G., Hauet, T., Girard, J. P., Gombert, J. M., Herbelin, A., & Thierry, A. (2018). Endogenous IL-33 contributes to kidney ischemia-reperfusion injury as an alarmin. *Journal of the American Society of Nephrology*, **29**(4), 1272–1288.

Florens, N., Kasam, R. K., Rudman-Melnick, V., Lin, S. C., Prasad, V., & Molkentin, J. D. (2023). Interleukin-33 mediates cardiomyopathy after acute kidney injury by signaling to cardiomyocytes. *Circulation*, **147**(9), 746–758.

Garner, K. L., Bowdridge, E. C., Griffith, J. A., DeVallance, E., Seman, M. G., Engels, K. J., Groth, C. P., Goldsmith, W. T., Wix, K., Batchelor, T. P., & Nurkiewicz, T. R. (2022). Maternal nanomaterial inhalation exposure, critical gestational period in the uterine microcirculation is angiotensin II dependent. *Cardiovascular Toxicology*, **22**(2), 167–180.

Ghali, R., Altara, R., Louch, W. E., Cataliotti, A., Mallat, Z., Kaplan, A., Zouein, F. A., & Booz, G. W. (2018). IL-33 (Interleukin 33)/sST2 axis in hypertension and heart failure. *Hypertension*, **72**(4), 818–828.

Ghouleh, I. A., Sahoo, S., Meijles, D. N., Amaral, J. H., de Jesus, D. S., Sembrat, J., Rojas, M., Goncharov, D. A., Goncharova, E. A., & Pagano, P. J. (2017). Endothelial Nox1 oxidase assembly in human pulmonary arterial hypertension; driver of Gremlin1-mediated proliferation. *Clinical Science (London, England, 1979)*, **131**(15), 2019–2035.

Gluck, J., Rymarczyk, B., & Rogala, B. (2012). Serum IL-33 but not ST2 level is elevated in intermittent allergic rhinitis and is a marker of the disease severity. *Inflammation Research*, **61**(6), 547–550.

Griesenauer, B., Jiang, H., Yang, J., Zhang, J., Ramadan, A. M., Egbosiuba, J., Campa, K., & Paczesny, S. (2019). ST2/MyD88 deficiency protects mice against acute graft-versus-host disease and spares regulatory T cells. *Journal of Immunology*, **202**(10), 3053–3064.

Huang, R., Li, L., Guo, H., & Wang, C. L. (2003). Caldesmon binding to actin is regulated by calmodulin and phosphorylation via different mechanisms. *Biochemistry*, **42**(9), 2513–2523.

Iijima, K., Kobayashi, T., Hara, K., Kephart, G. M., Ziegler, S. F., McKenzie, A. N., & Kita, H. (2014). IL-33 and thymic stromal lymphopoietin mediate immune pathology in response to chronic airborne allergen exposure. *Journal of Immunology*, **193**(4), 1549–1559.

Je, H. D., Gangopadhyay, S. S., Ashworth, T. D., & Morgan, K. G. (2001). Calponin is required for agonist-induced signal transduction–evidence from an antisense approach in ferret smooth muscle. *The Journal of Physiology*, **537**(Pt 2), 567–577.

Jiang, M. J., & Morgan, K. G. (1989). Agonist-specific myosin phosphorylation and intracellular calcium during isometric contractions of arterial smooth muscle. *Pflugers Archiv, European journal of physiology*, **413**(6), 637–643.

Katwa, P., Wang, X., Urankar, R. N., Podila, R., Hilderbrand, S. C., Fick, R. B., Rao, A. M., Ke, P. C., Wingard, C. J., & Brown, J. M. (2012). A carbon nanotube toxicity paradigm driven by mast cells and the IL-(3)(3)/ST(2) axis. *Small*, **8**(18), 2904–2912.

Kauffenstein, G., Drouin, A., Thorin-Trescases, N., Bachelard, H., Robaye, B., D'Orleans-Juste, P., Marceau, F., Thorin, E., & Sevigny, J. (2010). NTPDase1 (CD39) controls nucleotide-dependent vasoconstriction in mouse. *Cardiovascular Research*, **85**(1), 204–213.

Kim, H. R., Gallant, C., & Morgan, K. G. (2013). Regulation of PKC autophosphorylation by calponin in contractile vascular smooth muscle tissue. *BioMed research international*, **2013**, 358643.

Kindle, L., Rothe, L., Kriss, M., Osdoby, P., & Collin-Osdoby, P. (2006). Human microvascular endothelial cell activation by IL-1 and TNF-alpha stimulates the adhesion and trans-endothelial migration of circulating human CD14+ monocytes that develop with RANKL into functional osteoclasts. *Journal of Bone and Mineral Research*, **21**(2), 193–206.

Lan, J., Luo, H., Wu, R., Wang, J., Zhou, B., Zhang, Y., Jiang, Y., & Xu, J. (2020). Internalization of HMGB1 (High Mobility Group Box 1) promotes angiogenesis in endothelial cells. *Arteriosclerosis, Thrombosis, and Vascular Biology*, **40**(12), 2922–2940.

LaValley, D. J., Zanotelli, M. R., Bordeleau, F., Wang, W., Schwager, S. C., & Reinhart-King, C. A. (2017). Matrix stiffness enhances VEGFR-2 Internalization, signaling, and proliferation in endothelial cells. *Convergent Science Physical Oncology*, **3**, 044001.

Lee, C. H., Poburko, D., Sahota, P., Sandhu, J., Ruehlmann, D. O., & van Breemen, C. (2001). The mechanism of phenylephrine-mediated [Ca(2+)](i) oscillations underlying tonic contraction in the rabbit inferior vena cava. *The Journal of Physiology*, **534**(Pt 3), 641–650.

Lefrancais, E., & Cayrol, C. (2012). Mechanisms of IL-33 processing and secretion, differences and similarities between IL-1 family members. *European Cytokine Network*, **23**(4), 120–127.

Lefrancais, E., Duval, A., Mirey, E., Roga, S., Espinosa, E., Cayrol, C., & Girard, J. P. (2014). Central domain of IL-33 is cleaved by mast cell proteases for potent activation of group-2 innate lymphoid cells. *Proceedings of the National Academy of Sciences*, **111**(43), 15502–15507.

Lefrancais, E., Roga, S., Gautier, V., Gonzalez-de-Peredo, A., Monsarrat, B., Girard, J. P., & Cayrol, C. (2012). IL-33 is processed into mature bioactive forms by neutrophil elastase and cathepsin G. *Proceedings of the National Academy of Sciences*, **109**(5), 1673–1678.

Leinweber, B. D., Leavis, P. C., Grabarek, Z., Wang, C. L., & Morgan, K. G. (1999). Extracellular regulated kinase (ERK) interaction with actin and the calponin homology (CH) domain of actin-binding proteins. *Biochemical Journal*, **344**(Pt 1), 117–123.

Li, Y., Cifuentes-Pagano, E., DeVallance, E. R., de Jesus, D. S., Sahoo, S., Meijles, D. N., Koes, D., Camacho, C. J., Ross, M., St Croix, C., & Pagano, P. J. (2019). NADPH oxidase 2 inhibitors CPP11G and CPP11H attenuate endothelial cell inflammation & vessel dysfunction and restore mouse hind-limb flow. *Redox Biology*, **22**, 101143.

Li, Y., Kracun, D., Dustin, C. M., El Massry, M., Yuan, S., Goossen, C. J., DeVallance, E. R., Sahoo, S., St Hilaire, C., Gurkar, A. U., Finkel, T., Straub, A. C., Cifuentes-Pagano, E., & Pagano, P. J. (2021). Forestalling age-impaired angiogenesis and blood flow by targeting NOX, Interplay of NOX1, IL-6, and SASP in propagating cell senescence. *Proceedings of the National Academy of Sciences*, **118**(42), e2015666118.

Liu, Z., & Khalil, R. A. (2018). Evolving mechanisms of vascular smooth muscle contraction highlight key targets in vascular disease. *Biochemical Pharmacology*, **153**, 91–122.

Lohman, A. W., Billaud, M., & Isakson, B. E. (2012). Mechanisms of ATP release and signalling in the blood vessel wall. *Cardiovascular Research*, **95**(3), 269–280.

Luthi, A. U., Cullen, S. P., McNeela, E. A., Duriez, P. J., Afonina, I. S., Sheridan, C., Brumatti, G., Taylor, R. C., Kersse, K., Vandenabeele, P., Lavelle, E. C., & Martin, S. J. (2009). Suppression of interleukin-33 bioactivity through proteolysis by apoptotic caspases. *Immunity*, **31**(1), 84–98.

Moussion, C., Ortega, N., & Girard, J. P. (2008). The IL-1-like cytokine IL-33 is constitutively expressed in the nucleus of endothelial cells and epithelial cells in vivo, a novel 'alarmin'? *PLoS ONE*, **3**(10), e3331.

Nichols, C. E., Shepherd, D. L., Hathaway, Q. A., Durr, A. J., Thapa, D., Abukabda, A., Yi, J., Nurkiewicz, T. R., & Hollander, J. M. (2018). Reactive oxygen species damage drives cardiac and mitochondrial dysfunction following acute nano-titanium dioxide inhalation exposure. *Nanotoxicology*, **12**(1), 32–48.

Novelli, E. M., Little-Ihrig, L., Knupp, H. E., Rogers, N. M., Yao, M., Baust, J. J., Meijles, D., St Croix, C. M., Ross, M. A., Pagano, P. J., DeVallance, E. R., Miles, G., Potoka, K. P., Isenberg, J. S., & Gladwin, M. T. (2019). Vascular TSP1-CD47 signaling promotes sickle cell-associated arterial vasculopathy and pulmonary hypertension in mice. *American Journal of Physiology-Lung Cellular and Molecular Physiology*, **316**(6), L1150–L1164.

Nurkiewicz, T. R., Porter, D. W., Barger, M., Castranova, V., & Boegehold, M. A. (2004). Particulate matter exposure impairs systemic microvascular endothelium-dependent dilation. *Environmental Health Perspectives*, **112**(3), 1299–1306.

Nurkiewicz, T. R., Porter, D. W., Barger, M., Millecchia, L., Rao, K. M., Marvar, P. J., Hubbs, A. F., Castranova, V., & Boegehold, M. A. (2006). Systemic microvascular dysfunction and inflammation after pulmonary particulate matter exposure. *Environmental Health Perspectives*, **114**(3), 412–419.

Nurkiewicz, T. R., Porter, D. W., Hubbs, A. F., Cumpston, J. L., Chen, B. T., Frazer, D. G., & Castranova, V. (2008). Nanoparticle inhalation augments particle-dependent systemic microvascular dysfunction. *Particle and Fibre Toxicology*, **5**, 1.

Nurkiewicz, T. R., Porter, D. W., Hubbs, A. F., Stone, S., Chen, B. T., Frazer, D. G., Boegehold, M. A., & Castranova, V. (2009). Pulmonary nanoparticle exposure disrupts systemic microvascular nitric oxide signaling. *Toxicological Sciences*, **110**(1), 191–203.

Ozturan, A., Eyigor, H., Eyigor, M., Osma, U., Yilmaz, M. D., Selcuk, O. T., Renda, L., & Gultekin, M. (2017). The role of IL-25 and IL-33 in chronic rhinosinusitis with or without nasal polyps. *European Archives of Oto-Rhino-Laryngology*, **274**(1), 283–288.

Pan, D., Buchheit, K. M., Samuchiwal, S. K., Liu, T., Cirka, H., Raff, H., & Boyce, J. A. (2019). COX-1 mediates IL-33-induced extracellular signal-regulated kinase activation in mast cells, Implications for aspirin sensitivity. *Journal of Allergy and Clinical Immunology*, **143**(3), 1047–1057. e1048.

Park, J. H., Jin, Y. M., Hwang, S., Cho, D. H., Kang, D. H., & Jo, I. (2013). Uric acid attenuates nitric oxide production by decreasing the interaction between endothelial nitric oxide synthase and calmodulin in human umbilical vein endothelial cells, A mechanism for uric acid-induced cardiovascular disease development. *Nitric Oxide*, **32**, 36–42.

Patchell, V. B., Vorotnikov, A. V., Gao, Y., Low, D. G., Evans, J. S., Fattoum, A., El-Mezgueldi, M., Marston, S. B., & Levine, B. A. (2002). Phosphorylation of the minimal inhibitory region at the C-terminus of caldesmon alters its structural and actin binding properties. *Biochimica Et Biophysica Acta*, **1596**(1), 121–130.

Pentz, R., Kaun, C., Thaler, B., Stojkovic, S., Lenz, M., Krychtiuk, K. A., Zuckermann, A., Huber, K., Wojta, J., Hohensinner, P. J., & Demyanets, S. (2018). Cardio-protective cytokine interleukin-33 is up-regulated by statins in human cardiac tissue. *Journal of Cellular and Molecular Medicine*, **22**(12), 6122–6133.

Rodrigues, M., Kosaric, N., Bonham, C. A., & Gurtner, G. C. (2019). Wound healing, a cellular perspective. *Physiological Reviews*, **99**(1), 665–706.

Roussel, L., Erard, M., Cayrol, C., & Girard, J. P. (2008). Molecular mimicry between IL-33 and KSHV for attachment to chromatin through the H2A-H2B acidic pocket. *European Molecular Biology Organization Reports*, **9**(10), 1006–1012.

Salerno, J. C., Ghosh, D. K., Razdan, R., Helms, K. A., Brown, C. C., McMurry, J. L., Rye, E. A., & Chrestensen, C. A. (2014). Endothelial nitric oxide synthase is regulated by ERK phosphorylation at Ser602. *Bioscience Reports*, **34**(5), e00137.

Salmeron, K., Aihara, T., Redondo-Castro, E., Pinteaux, E., & Bix, G. (2016). IL-1alpha induces angiogenesis in brain endothelial cells in vitro, implications for brain angiogenesis after acute injury. *Journal of Neurochemistry*, **136**(3), 573–580.

Sanada, S., Hakuno, D., Higgins, L. J., Schreiter, E. R., McKenzie, A. N., & Lee, R. T. (2007). IL-33 and ST2 comprise a critical biomechanically induced and cardio-protective signaling system. *Journal of Clinical Investigation*, **117**(6), 1538–1549.

Song, Y. Y., Liang, D., Liu, D. K., Lin, L., Zhang, L., & Yang, W. Q. (2023). The role of the ERK signaling pathway in promoting angiogenesis for treating ischemic diseases. *Frontiers in Cell and Developmental Biology*, **11**, 1164166.

Stapleton, P. A., Minarchick, V. C., Yi, J., Engels, K., McBride, C. R., & Nurkiewicz, T. R. (2013). Maternal engineered nanomaterial exposure and fetal microvascular function, does the Barker hypothesis apply? *American Journal of Obstetrics and Gynecology*, **209**(227), e221–e211.

Sun, D., Meng, T. T., Loong, T. H., & Hwa, T. J. (2004). Removal of natural organic matter from water using a nano-structured photocatalyst coupled with filtration membrane. *Water Science and Technology*, **49**(1), 103–110.

Suttiponparnit, K., Jiang, J., Sahu, M., Suvachittanont, S., Charinpanitkul, T., & Biswas, P. (2011). Role of surface area, primary particle size, and crystal phase on titanium dioxide nanoparticle dispersion properties. *Nanoscale Research Letters*, **6**, 27.

Talabot-Ayer, D., Lamacchia, C., Gabay, C., & Palmer, G. (2009). Interleukin-33 is biologically active independently of caspase-1 cleavage. *Journal of Biological Chemistry*, **284**(29), 19420–19426.

Travers, J., Rochman, M., Miracle, C. E., Habel, J. E., Brusilovsky, M., Caldwell, J. M., Rymer, J. K., & Rothenberg, M. E. (2018). Chromatin regulates IL-33 release and extracellular cytokine activity. *Nature Communications*, **9**, 3244.

Turner, S. R., Chappellaz, M., Popowich, B., Wooldridge, A. A., Haystead, T. A. J., Cole, W. C., & MacDonald, J. A. (2019). Smoothelin-like 1 deletion enhances myogenic reactivity of mesenteric arteries with alterations in PKC and myosin phosphatase signaling. *Scientific Reports*, **9**, 481.

Turnquist, H. R., Zhao, Z., Rosborough, B. R., Liu, Q., Castellaneta, A., Isse, K., Wang, Z., Lang, M., Stolz, D. B., Zheng, X. X., Demetris, A. J., Liew, F. Y., Wood, K. J., & Thomson, A. W. (2011). IL-33 expands suppressive CD11b+ Gr-1(int) and regulatory T cells, including ST2L+ Foxp3+ cells, and mediates regulatory T cell-dependent promotion of cardiac allograft survival. *Journal of Immunology*, **187**(9), 4598–4610.

Wang, X., Katwa, P., Podila, R., Chen, P., Ke, P. C., Rao, A. M., Walters, D. M., Wingard, C. J., & Brown, J. M. (2011). Multi-walled carbon nanotube instillation impairs pulmonary function in C57BL/6 mice. *Particle and Fibre Toxicology*, **8**, 24.

Winder, S. J., & Walsh, M. P. (1993). Calponin, thin filament-linked regulation of smooth muscle contraction. *Cell-Signalling*, **5**(6), 677–686.

Winder, S. J., Walsh, M. P., Vasulka, C., & Johnson, J. D. (1993). Calponin-calmodulin interaction, properties and effects on smooth and skeletal muscle actin binding and actomyosin ATPases. *Biochemistry*, **32**(48), 13327–13333.

Yazji, I., Sodhi, C. P., Lee, E. K., Good, M., Egan, C. E., Afrazi, A., Neal, M. D., Jia, H., Lin, J., Ma, C., Branca, M. F., Prindle, T., Richardson, W. M., Ozolek, J., Billiar, T. R., Binion, D. G., Gladwin, M. T., & Hackam, D. J. (2013). Endothelial TLR4 activation impairs intestinal microcirculatory perfusion in necrotizing enterocolitis via eNOS-NO-nitrite signaling. *Proceedings of the National Academy of Sciences*, **110**(23), 9451–9456.

Yeh, Y. T., Hur, S. S., Chang, J., Wang, K. C., Chiu, J. J., Li, Y. S., & Chien, S. (2012). Matrix stiffness regulates endothelial cell proliferation through septin 9. *PLoS ONE*, **7**(10), e46889.

Zhu, Z., Peng, X., Li, X., Tu, T., Yang, H., Teng, S., Zhang, W., Xing, Z., Tang, J., Hu, X., Fang, Z., & Zhou, S. (2020). HMGB1 impairs endothelium-dependent relaxation in diabetes through TLR4/eNOS pathway. *Federation of American Societies for Experimental Biology Journal*, **34**, 8641–8652.

Additional information

Data availability statement

All of the data that support the present study are accessible in the final published article or the supporting information.

Competing interests

The authors declare that they have no competing interests.

Author contributions

E.D., S.H., E.E.K. and T.R.N. were responsible for the study conception and design. E.D., E.B., K.G., J.G., M.S., T.B., M.V. and W.T.G. conducted experiments and collected data. E.D., S.H., E.E.K., W.T.G., M.V. and T.R.N. were responsible for data analysis and interpretation. E.D., L.B., E.E.K., S.H., M.S. and T.R.N. were responsible for figure preparation writing and editing. All authors have approved the final version of the manuscript submitted for publication and agree to be accountable for all aspects of the work. All persons designated as authors qualify for authorship, and all those who qualify for authorship are listed.

Funding

ED was supported by U54GM104942 and AHA 23CDA1038976. EEK was supported by HL153532, DK124510 and 19TPA34850089. TRN was supported by ES015022. EB was supported by GM104942. SH was supported by ES031253. Additional funding comprised AHA-CDA1038976 and U54GM104942 (ED), NOISH K01-OH012320 (EB), NIEHS

R01-ES031253 (SH), NIDDK R01-DK124510 and NHLBI R01-HL153532 (EEK), and NIEHS R01-ES015022 (TRN).

Keywords

endothelial function, ERK signaling, interleukin, smooth muscle constriction, vascular tone

Supporting information

Additional supporting information can be found online in the Supporting Information section at the end of the HTML view of the article. Supporting information files available:

Peer Review History
Supplemental Data